

Comparison of dust-to-gas ratios in luminous, ultraluminous, and hyperluminous infrared galaxies

M. Contini^{1,*} and T. Contini²

¹ School of Physics and Astronomy, Tel-Aviv University, Tel-Aviv, 69978 Israel

² Laboratoire d'Astrophysique de Toulouse et Tarbes (LA2T - UMR 5572), Observatoire Midi-Pyrénées, 14 avenue E. Belin, F-31400 Toulouse, France

The dates of receipt and acceptance should be inserted later

Key words galaxies: active - galaxies: starburst - infrared: galaxies - shock waves

The dust-to-gas ratios in three different samples of luminous, ultraluminous, and hyperluminous infrared galaxies are calculated by modelling their radio to soft X-ray spectral energy distributions (SED) using composite models which account for the photoionizing radiation from HII regions, starbursts, or AGNs, and for shocks. The models are limited to a set which broadly reproduces the mid-IR fine structure line ratios of local, IR bright, starburst galaxies. The results show that two types of clouds contribute to the IR emission. Those characterized by low shock velocities and low preshock densities explain the far-IR dust emission, while those with higher velocities and densities contribute to the mid-IR dust emission. Clouds with shock velocities of 500 km s^{-1} prevail in hyperluminous infrared galaxies. An AGN is found in nearly all of the ultraluminous infrared galaxies and in half of the luminous infrared galaxies of the sample. High IR luminosities depend on dust-to-gas ratios as high as ~ 0.1 by mass, however most hyperluminous IR galaxies show dust-to-gas ratios much lower than those calculated for the luminous and ultraluminous IR galaxies.

© WILEY-VCH Verlag GmbH & Co. KGaA, Weinheim

1 Introduction

Observations in the infrared (IR) have revealed galaxies with very high IR luminosities, up to $L_{\text{IR}} \sim 10^{13} L_{\odot}$ (Lutz et al. 1998; Laurent et al. 2000; Tran et al. 2001; Verma et al. 2002). The origin of this high IR luminosity is under investigation (Genzel et al. 1998; Rowan-Robinson 1992, 2000; Rigopoulou et al. 1999; Farrah et al. 2002; Verma et al. 2003; etc.). The main questions concern the type (such as HII galaxy, starburst nucleus galaxy, or active galactic nucleus (AGN)) of the IR bright and luminous galaxies, the source of dust illumination and heating by a photoionizing flux and/or collisional processes, the composition of dust ranging from relatively large silicate grains to small graphite, PAH, ices, etc. (Spoon et al. 2002).

Dust plays an important role in the understanding of the near and distant Universe (Schneider, Ferrara & Salvaterra 2004). Formation of grains in the ISM is extremely inefficient, the preferred sites being the atmospheres of evolved low mass ($M < 8 M_{\odot}$) stars from where it is transported into the ISM through stellar winds (Whittet 1992). However, at high redshifts, e.g. $z > 5$, the evolutionary time-scales of low-mass stars ($0.1 - 1 \text{ Gyr}$) start to be comparable with the age of the Universe. Type II supernovae are the only known dust sources with evolutionary time-scales shorter than the Hubble time. Dust enrichment of the ISM must have occurred primarily on considerably shorter time-scales in the ejecta of supernova explosions.

In the starburst environments and in the outflow regions of AGN, dust dominates the IR emission by reprocessing radiation from the primary source (stars and/or an active nucleus). Collisional processes which were found to be so important to explain the emission-line and continuum spectra (e.g. the strong high-ionization level line fluxes, the soft X-ray emission, strong heating of dust, radio synchrotron emission, etc.) from the nuclear and circumnuclear regions of AGNs, starbursts and HII regions (e.g. Contini & Viegas 2000) dominate the emitted radiation flux in mergers. Particularly, it was demonstrated that collisional heating of dust grains by gas in supersonic velocity regimes, leads to relatively high temperatures which could explain the IR flux between 3 and $1000 \mu\text{m}$ (the "IR bump") in the continuum spectral energy distribution (SED) of starburst galaxies (Contini & Contini 2003) and AGNs (Contini, Viegas & Prieto 2004).

Our aim is to test whether the IR luminosity is directly related to the amount of dust relative to gas, namely the dust-to-gas ratio (d/g) which can be considered as a key parameter in modelling galaxies revealing high dust formation regions and tracing stellar evolution.

We investigate three luminosity classes commonly used for IR luminous galaxies: hyper-, ultra-, and luminous infrared galaxies (HLIRGs, ULIRGs, and LIRGs, respectively) which correspond to $> 10^{13}$, $> 10^{12}$ and $> 10^{11} h_{65}^{-2} L_{\odot}$, according to the definition of Sanders & Mirabel (1996). Three samples are chosen as representative of the different luminosity classes: Farrah et al. (2002), Rigopoulou et al. (1999), and Verma et al. (2003). Only three galaxies from

* Corresponding author: e-mail: contini@post.tau.ac.il

the Verma et al. (2003) sample correspond to the definition of Sanders & Mirabel, the other showing lower IR luminosities belong to the IR bright galaxies. However, in the following we will refer to them together with the luminous IR galaxies among the LIRGs. The samples are briefly presented in Sect. 2.

The galaxies in the different samples are chosen only because they are IR luminous and not by their type (e.g. starburst, HII regions, AGN, etc) which, viceversa, we will try to find out by modelling. Galaxies are generally classified through the analysis of the SED of the continuum and of the absorption and emission bands of dust main components, e.g. silicates and PAHs (Spoon et al. 2002), on top of it. Diagnostic diagrams are generally used to distinguish between AGN and star forming regions on the basis of PAH to continuum intensity ratios (Genzel et al. 1998, Peeters et al 2004), of the ratio of the continuum flux at different wavelengths (Genzel & Cesarsky 2000), PAH to fine structure lines (FSL) (Genzel et al 1998) and FSL diagrams (Sturm et al 2002). However, recent observations of mid-IR AGN spectra by the *Spitzer* Space Telescope (Weedman et al. 2005) found no spectral parameters that unambiguously distinguish AGNs and starbursts based only on the slopes of the continuum spectra.

The IR luminosity of galaxies depends on both dust reprocessed radiation in the IR and bremsstrahlung from cool gas. Dust IR emission is usually analysed independently of bremsstrahlung which covers the whole radio - X-ray frequency range. Indeed, in the IR domain dust emission dominates, but the modelling of the SED requires the consistent calculation of gas and dust spectra (Sect. 3). Previous modelling of AGNs and starburst galaxies (Viegas, Contini & Contini 1999; Contini, Viegas & Prieto 2004) has shown that many different conditions coexist in each galaxy. The observed continuum and emission-line spectra account for all of them. Modelling the continuum SED by multi-cloud models, we will be able to determine the d/g ratios and the relative contribution of the different mechanisms which are at work in the IR luminous "active" galaxies : AGN, starbursts, supernova remnants, etc. The results are presented in Sect. 4, discussed in Sect. 5 and summarized in Sect. 6.

2 The samples

The sample of Verma et al. (2003) contains starburst regions that are optically obscured, therefore similar to dense star forming regions in ULIRGs and HLIRGs. The IR luminosities are between 10^9 and $10^{12} L_{\odot}$, except for IC 342 corresponding to $3.74 \cdot 10^7 L_{\odot}$ which will be used for comparison. We will check whether an active nucleus cannot be excluded in some of these starburst galaxies, leading to hybrid types.

ULIRGs dominate the local luminosity function of galaxies with $L > 10^{12} L_{\odot}$ (Sanders & Mirabel 1996 and references therein). Most of their bolometric luminosity is emitted in the far-IR (8-1000 μm) (Rigopoulou et al. 1999) and

Table 1 Characteristics of the galaxies

	type ^a	d^b (Mpc)	$\log L_{\text{IR}}$ (L_{\odot})
LIRGs :			
NGC 253	HII	3.27	10.23
IC 342	HII	0.45	7.57
II Zw 40	HII	10.5	9.3
M82	HII	2.7	10.18
NGC 3256	HII	37.95	11.4
NGC 3690	HII	41.64	11.53
NGC 4038/9	HII	21.9	10.65
NGC 4945	HII,Sy2	7.47	10.66
NGC 5236	HII	6.92	10.11
NGC 5253	HII	5.39	9.21
NGC 7552	HII,Liner	21.15	10.83
ULIRGs :			
Mrk 1014	QSO	652.3	12.50
UGC 5101	IrS	160.	11.94
Mrk 231	IrS	168.8	12.48
Mrk 273	IrS	148.	12.07
Arp 220	IrS	72.	12.11
NGC 6240	IrS	96.	11.78
HLIRGs :			
F00235+1024	nl	2320.	13.04 ^c
07380-2342	nl	1160.	13.34 ^c
F10026+4949	Sy1	4480.	13.81 ^c
F12509+3122	QSO	3120.	13.26 ^c
13279+3401	QSO	1714.	12.88 ^c
14026+4341	Sy1	1280.	12.90 ^c
F14218+3845	QSO	4840.	13.06 ^c
F16124+3241	nl	3381.	13.02 ^c
EJ1640+41	QSO	4400.	12.90 ^c
18216+6418	Sy1	1200.	13.14 ^c

^a from Verma et al. (2003) for LIRGs, Rigopoulou et al. (1999) for ULIRGs, and from Farrah et al. (2002) for HLIRGs.

^b adopting $H_0 = 75 \text{ km s}^{-1} \text{ Mpc}^{-1}$

^c 1-1000 μm luminosities obtained from the best-fitting combined starburst-AGN models (Farrah et al. 2002, table 3)

they show more prominent FIR emission than either starburst galaxies or AGNs (Peeters et al. 2004). Most ULIRGs are very rich in dust and gas, and they are interacting systems with distorted morphologies. Their optical spectra mimic those of Seyfert galaxies (Rigopoulou et al. 1999, Lutz et al. 1999). The MIR spectra of ULIRGs are more complicated than the spectra of other galaxies due to the presence of copious amount of dust in their nuclear regions (Genzel et al. 1998), leading to strong absorption features which may distort any emission component (Sturm et al. 2002).

Infrared, millimeter and radio characteristics of ULIRGs are similar to those of starburst galaxies, while nuclear optical emission-line spectra are similar to those of Seyfert galaxies. A central AGN and circumnuclear star formation may both play a role in the FIR emission (Rigopoulou et al 1999). At intermediate luminosities, some ULIRG spectra are PAH dominated, while others show signs of a 8 μm

broad peak, indicating the presence of deeply dust-enshrouded ionizing sources (Rigopoulou et al. 1999). On the other hand, the spectra at high FIR luminosities bear close resemblance to AGN hot dust continua, showing little or no sign of PAH features (Clavel et al. 2000). Of the ultraluminous IRAS selected in Sect. 3, galaxies, 70-80% are predominantly powered by recently formed massive stars, 20-30% by AGN (Genzel et al. 1998; Laurent et al. 2000). From multi-band HST imaging data Borne et al. (2001) find that ULIRGs show a significant population of very bright knots, which are most likely produced during the starburst/merger event.

At least some HST observations (Farrah et al. 2002) show that a small fraction of HLIRGs are merging galaxies. Mergers between evolved galaxies trigger dust enshrouded starburst and AGN activity (Sanders & Mirabel 1996). Alternatively, HLIRGs may be very young or even “primeval” galaxies (Rowan-Robinson 2000, Farrah et al. 2002). Rowan-Robinson argues that the bulk of emission in HLIRGs is due to starburst activity, implying star formation rates $> 1000 M_{\odot} \text{ yr}^{-1}$. Verma et al. (2002) and Farrah et al. (2002) claim that both starburst and AGN activities are required to explain the total IR emission, the average starburst fraction being 35%, within a range spanning from 80% starburst-dominated to 80% AGN-dominated.

The types, the distances from Earth calculated adopting $H_0 = 75 \text{ km s}^{-1} \text{ Mpc}^{-1}$, and the luminosities of the galaxies in the different samples are given in Table 1.

3 Modelling the spectra of starburst galaxies

We start by modelling the IR emission-line spectra observed by Verma et al. (2003) for a sample of starburst galaxies with relatively high IR fluxes and select the models (Sect. 3.1) which best explain the trend of the line ratios (Sect. 3.2), because line spectra are far more constraining than the SEDs. So we derive the grid of models suitable to model the SEDs (Sect. 3.3) by the method of Contini & Contini (2003) and Contini, Viegas & Prieto (2004) for different samples of luminous IR galaxies, and AGNs, respectively. Namely, gas and dust are heated and ionized consistently by photoionization and shocks (Sect. 3.4), so the ratio of dust reprocessed radiation to bremsstrahlung in the IR depends on d/g (Sect. 3.5).

3.1 The models

We use composite models which account consistently for photoionization from an external source and for shocks, in a plane-parallel geometry (see Contini & Contini 2003, Contini et al. 2004). Richtmyer-Meshkov instability between two fluids at different densities driven by shock waves and Kelvin-Helmholtz instability lead to perturbed circular material which is broken up into relatively small filaments. (Graham & Zhang 2000, Contini & Formigini 2001). The code SUMA (Viegas & Contini 1994, Contini & Contini 2003, Contini et

al. 2004, and references therein). is adopted for the calculations of the spectra. SUMA includes shock hydrodynamics which implies a leading role of collisional processes, as well as excitation and destruction of dust grains.

Other codes deal with dust emission in the IR, in particular GRASIL (Silva et al. 1998) and MAPPINGS (Groves et al. 2006 and references therein). GRASIL predicts time dependent SEDs of galaxies from X-ray to radio, including the effects of age selective extinction of stellar populations. The d/g ratio, assumed to scale linearly with the metallicity of the residual gas, determines the optical depth of the clouds. MAPPINGS adopts stochastic quantum heating of dust and a power-law size distribution of grains with index arising from shattering.

In our models the photoionizing flux from an AGN, F_{h} (in photons $\text{cm}^{-2} \text{ s}^{-1} \text{ eV}^{-1}$ at 1 Ryd), corresponds to a power-law. For starburst galaxies, the radiation flux from a star cluster of age (t) is characterized by the ionization parameter U . For HII regions, the radiation flux is a black body corresponding to the stellar colour temperature T_{\star} . The shocks, characterized by the shock velocity, V_s , the preshock density, n_0 , and the preshock magnetic field, B_0 ($= 10^{-4}$ gauss for all models), are created by collision of the ejected matter with the interstellar clouds. The abundance of He, C, N, O, Ne, Mg, Si, S, A, Cl, and Fe relative to H and the dust-to-gas ratio, d/g are also input parameters.

The clouds move outwards from the galaxy centre in the NLR of AGN (see e.g. Heckman et al. 1981), and in the neighbourhood of starbursts, therefore, the photoionizing flux and the shock act on the opposite edges of the clouds whose geometrical thickness, D , plays an important role in model results. The structure of the gas downstream is determined by the shock. Grains are sputtered depending on V_s and n_0 (Contini et al. 2004). The sputtering rate determines the distribution of the grain radius throughout a cloud. An initial grain radius $a_{\text{gr}} = 0.2 \mu\text{m}$ is generally adopted. Small grains ($\leq 0.2 \mu\text{m}$) deriving from sputtering of larger grains contribute in the integrated continuum SED.

It was found (Schneider et al. 2004) that for all but the smallest progenitor stars, silicate grains are the dominant dust compound. The characteristic grain sizes range between $10^{-3} \mu\text{m}$ and a few $\times 0.1 \mu\text{m}$, depending on the grain species and on the mass of the stellar progenitor. Very small grains are destroyed in regions of high UV radiation intensity (Rowan-Robinson 1992), so the maximum grain temperature which would account for the near-IR emission is limited by sublimation. Most of the grain survive in the narrow line region (NLR), where the the cloud velocities are $\sim 300\text{-}1000 \text{ km s}^{-1}$, while small grains ($< 0.1 \mu\text{m}$) are easily sputtered for shock velocities $\geq 200 \text{ km s}^{-1}$.

PAHs are responsible for no more than 22% of the total $3\text{-}1100 \mu\text{m}$ emission in normal galaxies (Dale et al. 2001). In the shock dominated starburst and AGN regions, small grains such as graphite and PAH are rapidly destroyed by sputtering, leading to an even lower percentage. Moreover, a strong radiation flux dilutes the PAHs which are hardly seen

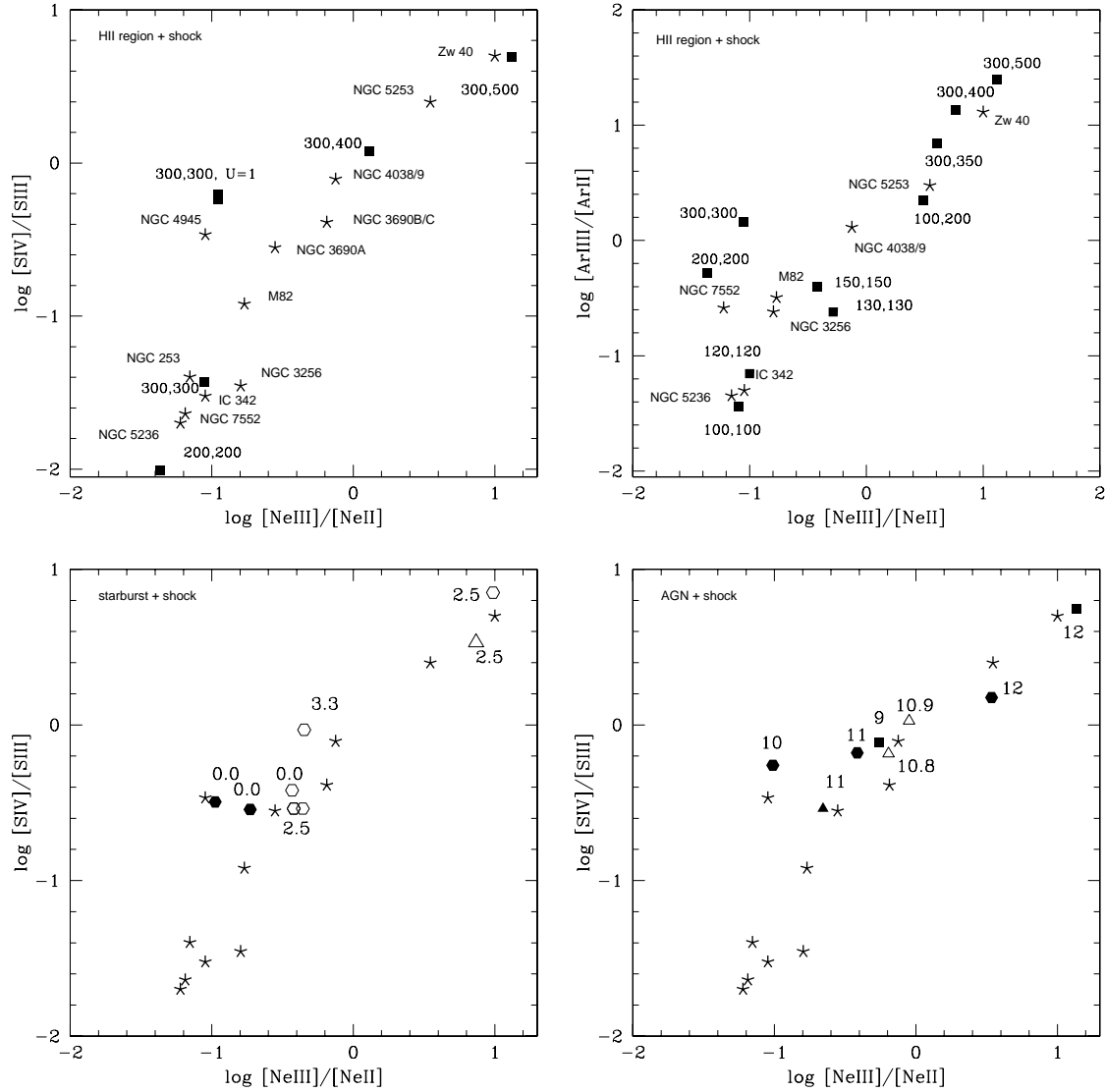


Fig. 1 *Top left:* comparison of observed line ratios $[SIV]/[SIII]$ vs. $[NeIII]/[NeII]$ (asterisks) with models for HII regions + shocks (filled squares). Values of V_s and n_0 are indicated near each model. *Top right:* comparison of observed line ratios $[ArIII]/[ArII]$ vs. $[NeIII]/[NeII]$ with models for HII regions + shocks. Same symbols as for top left diagram. *Bottom left:* comparison of observed line ratios $[SIV]/[SIII]$ vs. $[NeIII]/[NeII]$ (asterisks) with models for starbursts + shocks. Numbers refer to the starburst age in Myr. Open symbols represent geometrically thin clouds with $D = 0.03$ pc, filled symbols $D = 3$ pc; hexagons correspond to $V_s = 300$ km s $^{-1}$, $n_0 = 300$ cm $^{-3}$, triangles to $V_s = 200$ km s $^{-1}$, $n_0 = 200$ cm $^{-3}$. *Bottom right:* comparison of observed line ratios $[SIV]/[SIII]$ vs. $[NeIII]/[NeII]$ (asterisks) with models for AGN + shocks. Numbers represent $\log F_h$. filled triangles: $V_s = 200$ km s $^{-1}$, $n_0 = 200$, $D = 3$ pc; empty triangles: $V_s = 200$ km s $^{-1}$, $n_0 = 200$, $D = 0.3$ pc; black hexagons: $V_s = 300$ km s $^{-1}$, $n_0 = 300$, $D = 3$ pc; black squares: $V_s = 500$ km s $^{-1}$, $n_0 = 300$, $D = 3$ pc. All models except where indicated correspond to $U=10$.

in AGN (Sturm et al. 2000, 2002 and Laurent et al. 2000). PAH, with radius < 0.01 μ m survive only in the extended "cirrus" regions of starburst galaxies (see Contini & Contini 2003), and very seldom in the NLR of AGNs. Stochastic heating leads to temperature fluctuations around 20 K of $a_{gr}=200$ Å grains, but small grains ($a_{gr}=25$ Å) can reach 50 K and even 1000 K for $a_{gr}=5$ Å (Draine 2003). However, their contribution to the IR is negligible because the cirrus region is located in the edges of the extended underlying

galaxy, where d/g is even lower than in the ISM. So only silicate are accounted for in our models.

3.2 The line ratios

Verma et al. (2003) present ISO Short Wavelength Spectrometer (SWS) spectra between 2.38 and 45 μ m for 12 starburst regions located in eleven galaxies with $10^9 L_\odot < L_{IR} < 10^{12} L_\odot$. Radio and infrared measurements demon-

Table 2 Single-cloud models (top), the fluxes (in $\text{erg cm}^{-2} \text{s}^{-1}$) calculated in the different ranges (middle) and the maximum temperature of the grains (bottom); V_s : the shock velocity, n_0 : the preshock density, D : the geometrical thickness of the cloud, U : the ionization parameter, d/g : the dust-to-gas ratio, F_h : the ionization power-law ($\alpha=1.5$) flux (in number of photons $\text{cm}^{-2} \text{s}^{-1} \text{eV}^{-1}$ at 1 Ryd), $F_{radio_{br}}$: the radio flux calculated by bremsstrahlung, $F_{IR_{br}}$: the IR flux calculated by bremsstrahlung, $F_{opt_{br}}$: the optical flux calculated by bremsstrahlung, $F_{UV_{br}}$: the UV flux calculated by bremsstrahlung, F_{IR_d} : the IR flux calculated by dust, $T_d(\text{max})$ (K): the maximum temperature of grains. $T_*=10^4$ K is used for models m1-m5.

	<i>under- gal</i>		<i>starbursts</i>				<i>winds</i>	<i>AGN</i>
	m0	m1	m2	m3	m4	m5	m6	m7 ^a
$V_s(\text{km s}^{-1})$	100	150	200	250	300	500	1000	1000
$n_0 (\text{cm}^{-3})$	1000	100	200	300	300	300	300	1000
$D (10^{19} \text{ cm})$	1.e-4	1.e-4	1.	1.	0.5	1.	0.01	0.1
U	-	0.1	10	10	10	10	-	$\log F_h = 11$
$d/g (0.04)^b$	0.01	0.003	1.	1.	1.	1.	1.	0.1
$F_{radio_{br}}$	7.6e-6	3.2e-9	0.023	0.14	0.037	0.22	6.3e-6	6.6
$F_{IR_{dust}}$	0.01	3.2e-4	1.5e3	5.8e3	694.	1.23e4	819.	3.6e4
$F_{IR_{br}}$	5.4e-3	5.8e-6	13.2	71.	32.4	100.	0.01	6.0e3
$F_{opt_{br}}$	2.3e-4	5.5e-6	1.7	2.9	14.2	0.2	0.015	2.7e3
$F_{UV_{br}}$	6.e-4	2.e-5	0.195	0.14	11.6	31.	0.076	4.9e3
$F_{X_{br}}$	-	4.3e-7	2.2e-3	2.6e-3	0.018	1.	8.27	1.36
$T_d(\text{max})$ (K)	63.2	51.5	50.	82.	90.	119.	174.	155.

^a calculated with $a_{gr} = 1 \mu\text{m}$; ^b by mass

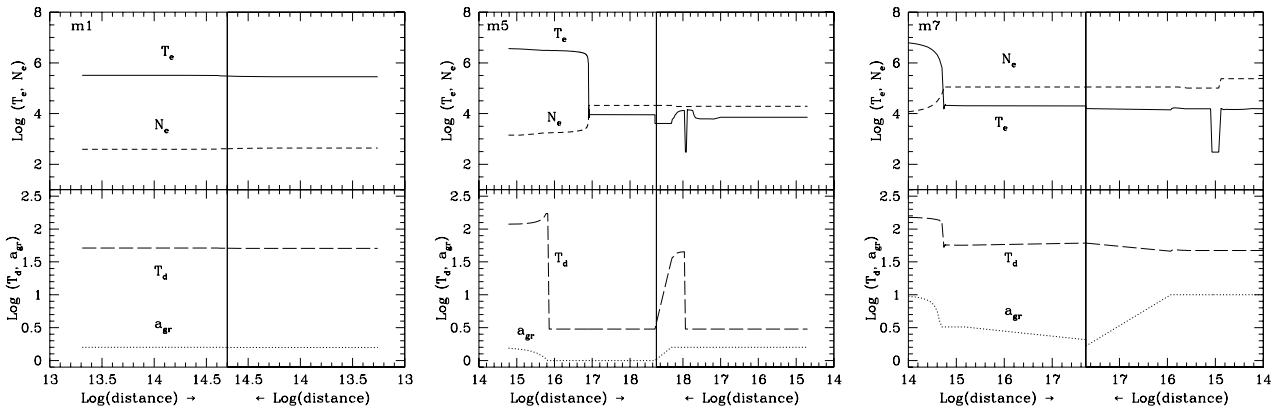


Fig. 2 The profile of the electron temperature, T_e , of the electron density, N_e , of the grain temperature, T_d , and of the grain radius, a_{gr} , throughout a cloud for models m1 (left), m5 (middle), and m7 (right).

strate that some of the most active star-forming regions are optically obscured, with most of the bolometric luminosity emerging in the IR.

We analyse the spectra observed by Verma et al. (2003, table 2) using the grids of models presented by Contini & Viegas (2001a,b). We focus on the ratios of MIR fine structure line transitions relative to Ne, S, and Ar. These elements, in fact, appear in at least two ionization levels. C, Si, and Fe etc., which are important in tracing dusty regions, as they can be trapped into dust grains and depleted from the gaseous phase, correspond to only one level.

We have chosen line ratios belonging to the same element and corresponding to different ionization levels, which do not depend on the relative abundances, but only on the physical parameters. Indeed the relative abundances of the

most coolant elements can influence the line ratios calculated with a given model, changing the distribution of the ion fractional abundance downstream. However, we are dealing here with neon, sulfur, and argon which are not important coolants. Moreover, Verma et al. (2003) conclude that Ne and Ar are overabundant by no more than a factor of ~ 3 relative to the solar ones, while S is underabundant by a similar factor (see also Contini & Contini 2003). We adopt cosmic abundances (Allen 1973).

The $[\text{SIV}]10.5/[\text{SIII}]18.7$ versus $[\text{NeIII}]15.55/[\text{NeII}]12.8$ emission-line ratios observed in starburst galaxies are compared in Fig. 1 (top left) with models calculated using a black body radiation flux which corresponds to HII regions and shocks. The models which best reproduce the data were calculated (Contini & Viegas 2001b) with a stellar colour

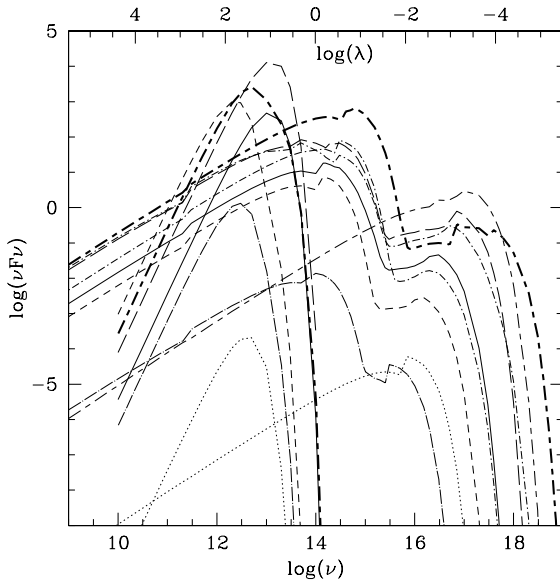


Fig. 3 Comparison of the model SEDs : m0 (long dash - dotted), m1 (dotted lines), m2 (short dashed), m3 (dot - short dashed), m4 (solid), m5 (long dashed), m6 (thin long dash - short dashed), and m7 (thick long dash - short dashed).

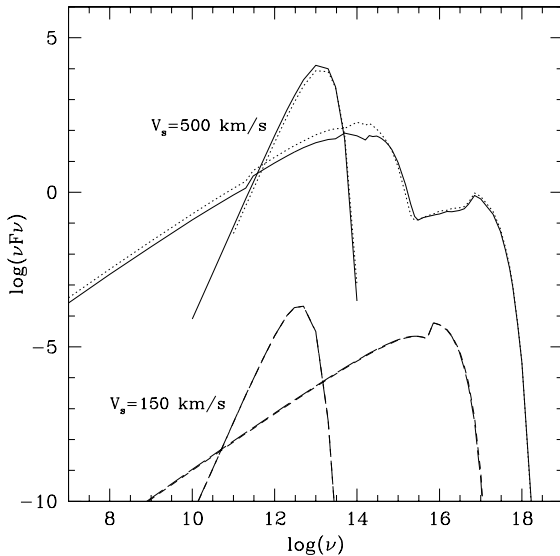


Fig. 4 Comparison of continua calculated using models which account i) for a black-body flux with $U = 10$ (long-dashed lines for $V_s = 150 \text{ km s}^{-1}$, and solid lines for $V_s = 500 \text{ km s}^{-1}$), and ii) for a power-law flux with $\log(F_h) = 10$ (short-dashed lines for $V_s = 150 \text{ km s}^{-1}$ and dotted lines for $V_s = 500 \text{ km s}^{-1}$)

temperatures $T_* = 10,000 \text{ K}$, a ionization parameter $U = 10$, and a geometrical thickness of 3 pc . The relatively high U indicates that the emitting clouds are close to the stars. Only NGC 4945 is explained by lower fluxes ($U \sim 1$). The observed line ratios (asterisks) follow the trend of models with increasing n_0 and V_s which are indicated near each model. Higher V_s in young starbursts, e.g. for II Zw 40, can be related to strong stellar winds produced by young massive stars (e.g. Wolf-Rayet stars).

In Fig. 1 (bottom left), the $[\text{SIV}] 10.5 / [\text{SIII}] 18.7$ versus $[\text{NeIII}] 15.55 / [\text{NeII}] 12.8$ observed line ratios are compared with models (Contini & Viegas 2001b) which take into account black-body radiation from stars with a temperature distribution corresponding to that of a cluster with a certain age. The emitting gas is ionized and heated by radiation from the stars and by shocks. Only galaxies showing $[\text{SIV}]/[\text{SIII}] > 0.15$ are explained by starburst models. The emitting clouds are mostly geometrically thin ($D \leq 0.03 \text{ pc}$), and the best fitting models were calculated with $U \leq 0.1$, indicating that the clouds are rather far from the radiation source, and/or that the sources are relatively weak. The starburst ages in Myr are indicated near each model. Galaxies with line ratios > 0.1 correspond generally to young ages ($t = 0.0 - 2.5 \text{ Myr}$), with a maximum of $t = 3.3 \text{ Myr}$ for NGC 4038/4039. However, there is no clear trend between the observed line ratios and starburst ages or shock velocities. The shock velocities are generally of the order of $200\text{-}300 \text{ km s}^{-1}$.

In Fig. 1 (bottom right) the galaxy sample is compared with models which account for radiation from an AGN and shocks. Also in these case the galaxies with low $[\text{SIV}]/[\text{SIII}]$ cannot be explained by the models, while there is a rough trend of higher line ratios corresponding to higher flux intensity, F_h from the active centre.

Fig. 1 (top left) shows that models calculated for HII regions explain the line ratios of all the sample galaxies. For sake of consistency, we have applied the same models to $[\text{ArIII}] 8.99 / [\text{ArII}] 6.99$ versus $[\text{NeIII}] 15.5 / [\text{NeII}] 12.8$ diagrams (Fig. 1 top right). Indeed, the models fit the observational data well. The distribution of the galaxies in the diagram is not very different from that corresponding to $[\text{SIV}]/[\text{SIII}]$ versus $[\text{NeIII}]/[\text{NeII}]$, and can be explained by the same shock velocity trend.

The starburst galaxies observed by Verma et al. (2003) also appear in the sample of Lutz et al (1998). In a previous analysis by Viegas, Contini, & Contini (1999), the modelling of II Zw 40 and NGC 5253 led to gas with low V_s and n_0 , in agreement with their young age, on the basis of high $[\text{OIV}]/([\text{NeII}] + 0.44[\text{NeIII}])$ versus $[\text{NeIII}]/[\text{NeII}]$ line ratios. However, in the analysis of $[\text{SIV}]/[\text{SIII}]$, we find that the same two galaxies are explained by HII region clouds with relatively high V_s (500 km s^{-1}), by clouds in starbursts with an age of $\sim 2.5 \text{ Myr}$ and velocities of $200\text{-}300 \text{ km s}^{-1}$, and by clouds in AGNs with velocities of $\sim 300 \text{ km s}^{-1}$.

Recall that ionization potentials of sulphur are lower than those of the corresponding levels of oxygen, therefore

the stratification downstream of S^{+3} and S^{+2} ions is different than that of O^{+3} , Ne^{+2} , and Ne^{+1} . The ionization potentials of sulphur are also lower than those of the corresponding levels of argon, therefore the stratification downstream of the S^{+3} and S^{+2} ions corresponds roughly to that of Ar^{+2} and Ar^{+1} . Therefore, the two top diagrams of Fig. 1 show similar results, which are reasonably different from those obtained from the $[OIV]/([NeII]+0.44[NeIII])$ analysis. This indicates that clouds in different physical conditions contribute to the different lines, e.g. $[SIV]$ and $[OIV]$, with various importance. Multi-cloud models were indeed suggested by Viegas et al. (1999, table 2) by modelling other galaxies of the sample, M 82, NGC 3256, and NGC 253, on the basis of infrared line ratios. Particularly, for M 82 the contribution of the models corresponding to $V_s=400$ $km\ s^{-1}$ and $100\ km\ s^{-1}$ is 0.82 and 0.13 to the $[OIV]25.9$ line, but it is 0.40 and 0.45, respectively, to $[NeIII] 15.5$.

Summarizing, the lines which appear in Fig. 1 diagrams are emitted by clouds located near the stars, which are characterized by temperatures of $T_* \sim 10\ 000$ K. Model results show that HII regions explain the $[SIV]/[SIII]$ line ratios for all the galaxies of the sample, in agreement with the galaxy spectral types given by Verma et al (2003, Table 1). Cluster of stars located in different regions of the galaxies also contribute, as well as an active nucleus in some galaxies. More particularly, the galaxies of the Verma et al. (2003) sample show that II Zw 40, NGC 5253, NGC 4038/4039, NGC 3690A and NGC 3690 B/C present a multiple nature of HII regions, AGN, and starburst galaxies.

3.3 The grid

From the current literature and from diagnostic diagrams (Fig. 1) it became evident that many mechanisms coexist in each galaxy. Therefore, the grid of selected models (Table 2) accounts for starbursts, AGN, HII regions, SNR winds, etc. We reduced the full set of models to a few prototypes to have clear results.

It is generally believed that starbursts characterize luminous IR galaxies because dust is formed in the atmosphere of massive stars. So the models suitable to the starburst clouds (m2-m5) show different physical parameters which were selected cross-checking the SEDs. An AGN, is often discovered in starburst galaxies, dominating the galactic central region where densities and velocities are relatively high, while the spectra emitted from shocked clouds in the external NLR of AGN is hardly distinguished from those emitted by clouds in the neighbourhood of starbursts. Therefore, we included in the grid only one model (m7) corresponding to the AGN, with large grains ($a_{gr} = 1\ \mu m$) which can survive sputtering downstream at relative high shock velocities and densities.

SNR are strong emitters of radio and X-ray downstream of strong shocks created by the SN explosion. We include in the grid model m6, a shock dominated model ($U=0$) with a relatively high velocity suitable to explain soft-X-ray observations.

Finally, the underlying galaxy spectra must be taken into account, represented by models showing a lower V_s , a low geometrical thickness, D due to the fragmentary character of the clouds, and a diluted photoionizing flux from the source. We have added to the grid model m0 ($d/g = 4 \cdot 10^{-4}$) which was found necessary to reproduce the MIR continuum of most of the galaxies in the Alonso-Herrero et al. (2003) sample (Contini, Viegas & Prieto 2004). The d/g values in the underlying galaxy are typical of the ISM.

The models (Contini & Viegas (2001a,b) adopted to explain the line ratios, were calculated assuming dust-to-gas ratios of $4 \cdot 10^{-5}$ by mass, which are low, even compared to the Galactic ISM ($d/g \sim 4 \times 10^{-4}$). By combining these models to fit the continuum SED, more realistic d/g ratios will be obtained.

The comparison of calculated with observed SEDs indicates that the best agreement is obtained by d/g higher by some orders of magnitude in all the models, except in those corresponding to low V_s (100-150 $km\ s^{-1}$) and low n_0 (100 cm^{-3}). The models with $V_s \geq 200\ km\ s^{-1}$ recalculated adopting a more suitable d/g however, could not explain the observed line ratios (Figs. 1), indicating that the line spectra are emitted from gas less obscured by dust and that dust is not distributed homogeneously throughout a galaxy. Lines emitted from the dusty regions are weak compared to those emitted from dust-free ones because a high d/g speeding up the cooling rate, reduces the ion fractional abundances by recombination.

3.4 The single-cloud models

The calculated bremsstrahlung integrated throughout the radio, IR, optical, UV, and X-ray ranges for the different models, are given in rows 7, 9, 10, 11, and 12 of Table 2, respectively. In row 9 the calculated flux emitted in the IR by reprocessed dust, F_{IR_d} is shown for comparison. Notice that both bremsstrahlung and reradiation by dust increase with V_s , n_0 and U . Particularly, shock-dominated models (calculated with $U = 0$) such as m6 show very low bremsstrahlung radiation.

The maximum temperatures of the grains downstream are given in the last row of Table 2 (bottom). The temperatures increase with V_s . However, density and grain sputtering also affect the heating and cooling of dust. This can be noticed by comparing the maximum temperature of grains calculated with models m0 and m1.

The profiles of the temperature and density of the gas, and of the temperature and radius of dust grains calculated for models m1, m5, and m7 are shown in Fig. 2 (left, middle, and right diagrams, respectively) for comparison.

The left edge of the diagrams represents the shock front. Here collisional processes dominate the heating of dust and gas up to a certain distance downstream which is determined by the shock velocity and by the density. The grains are destroyed by sputtering in the region close to the shock front (middle and right diagrams). The photoionizing flux reaches the opposite edge, heating and ionizing gas and dust.

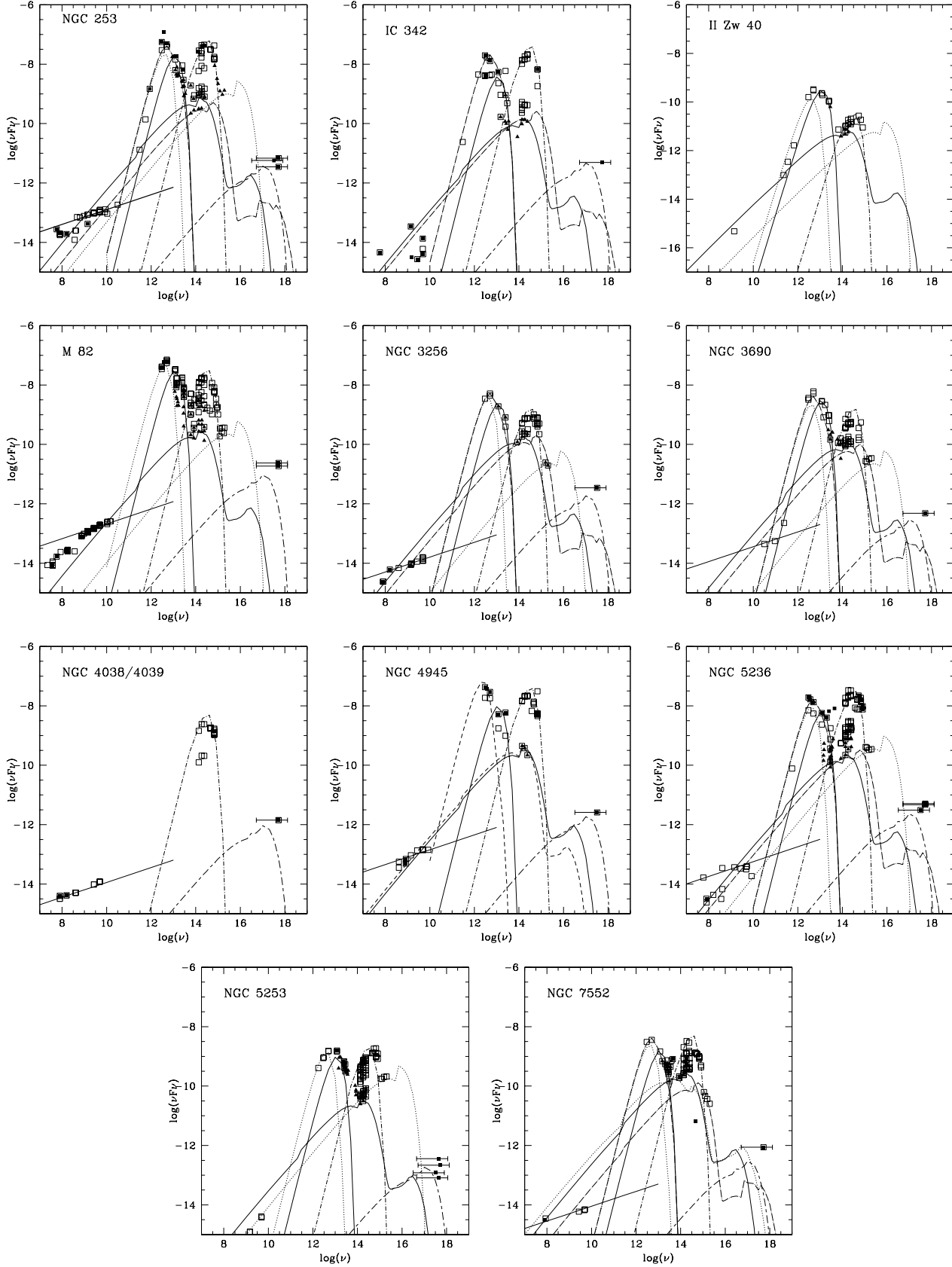


Fig. 5 Modelling the SEDs of the Verma et al. (2003) luminous IR galaxies sample. Black triangles: data from the NED. Black squares in the II Zw 40 diagram : data from Galliano (2004). Dotted lines: m1; short-dashed lines: m2-m3; solid lines: m4; long-dashed lines: m5; long dash-dot lines: m7; short-long-dashed lines: m6; dash-dotted line: bb model for the old star population; solid line: synchrotron radiation.

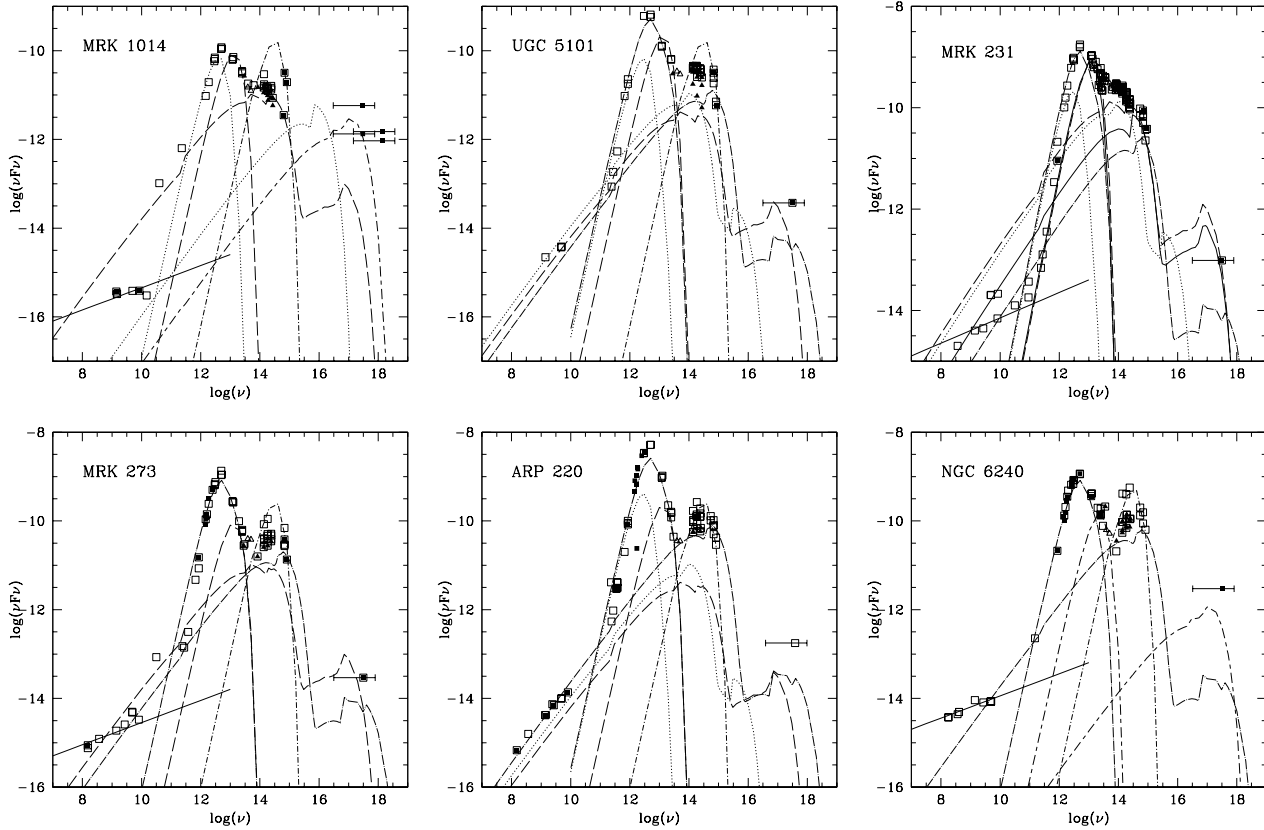


Fig. 6 Modelling the SED of the ULIRGs from the Rigopoulou et al. (1999) sample. Symbols as in Fig. 5. Empty triangles: Rigopoulou et al. (1999) IR data at 5.9 and 7.7 μm

The continuum SEDs calculated by models m0-m7 are compared in Fig. 3. Two curves correspond to each model, one representing dust reradiation and the other bremsstrahlung. The bremsstrahlung peak between 10^{13} and 10^{15} Hz depends on photoionization, while the maximum at higher frequencies is determined by the shock. For each model, the peak intensity of dust reprocessed radiation depends on d/g and the peak frequency on V_s . However, Fig. 3 shows that sputtering may change the distribution of the grains and shift the peak at lower frequencies (e.g. model m7). The MIR flux emitted by dust corresponding to $V_s = 300 \text{ km s}^{-1}$ and 500 km s^{-1} (models m4 and m5, respectively) show very similar SEDs, while the corresponding bremsstrahlung at frequencies $\geq 10^{13}$ Hz are different. Therefore, we will constrain the models by both the IR dust reradiation flux and the bremsstrahlung in the IR, optical, UV, and X-ray range.

The bremsstrahlung of models m6 and m7, both calculated with $V_s = 1000 \text{ km s}^{-1}$, show different distributions because m6 is shock dominated while m7 is radiation dominated. Moreover, they are calculated by different n_0 and different grain sizes.

The accuracy of the data in the optical-UV range is not high enough to select between power-law and black-body fluxes by modelling the continuum SED only (see also Contini & Viegas 2000, Fig. 1). Shock velocities instead can be estimated by the peak at high frequencies of bremsstrahlung

and by the frequency of the IR emission peak (Contini et al. 2004). A comparison of different models is shown in Fig. 4.

3.5 The continuum SED

3.5.1 Selection of the data

The data from the NED (NASA Extragalactic Database) are adopted for LIRGs, complemented with data from the literature to fulfil the dataset of ULIRGs and HLIRGs by Rigopoulou et al and Farrah et al., respectively. The data correspond to different apertures. In the diagrams we will distinguish between those taken with the smallest aperture (up to 14 arcseconds, black triangles), those with large apertures (white squares), and those integrated from maps (black squares). The observational errors are not shown in the diagrams in order to obtain less confused pictures.

All the data are important in modelling. Those taken with a large aperture cover different regions characterised by radiation from different sources in the same galaxy, therefore they correspond to multi-cloud models. This method led for example to the identification of the starbursts in the region close to the nucleus of the low luminosity AGN NGC 4579 (Contini 2004), or in the outskirts of NGC 7130 AGN (Contini et al. 2002). Data obtained with different apertures at frequencies close to silicate, PAH, graphite, ice, etc. bands

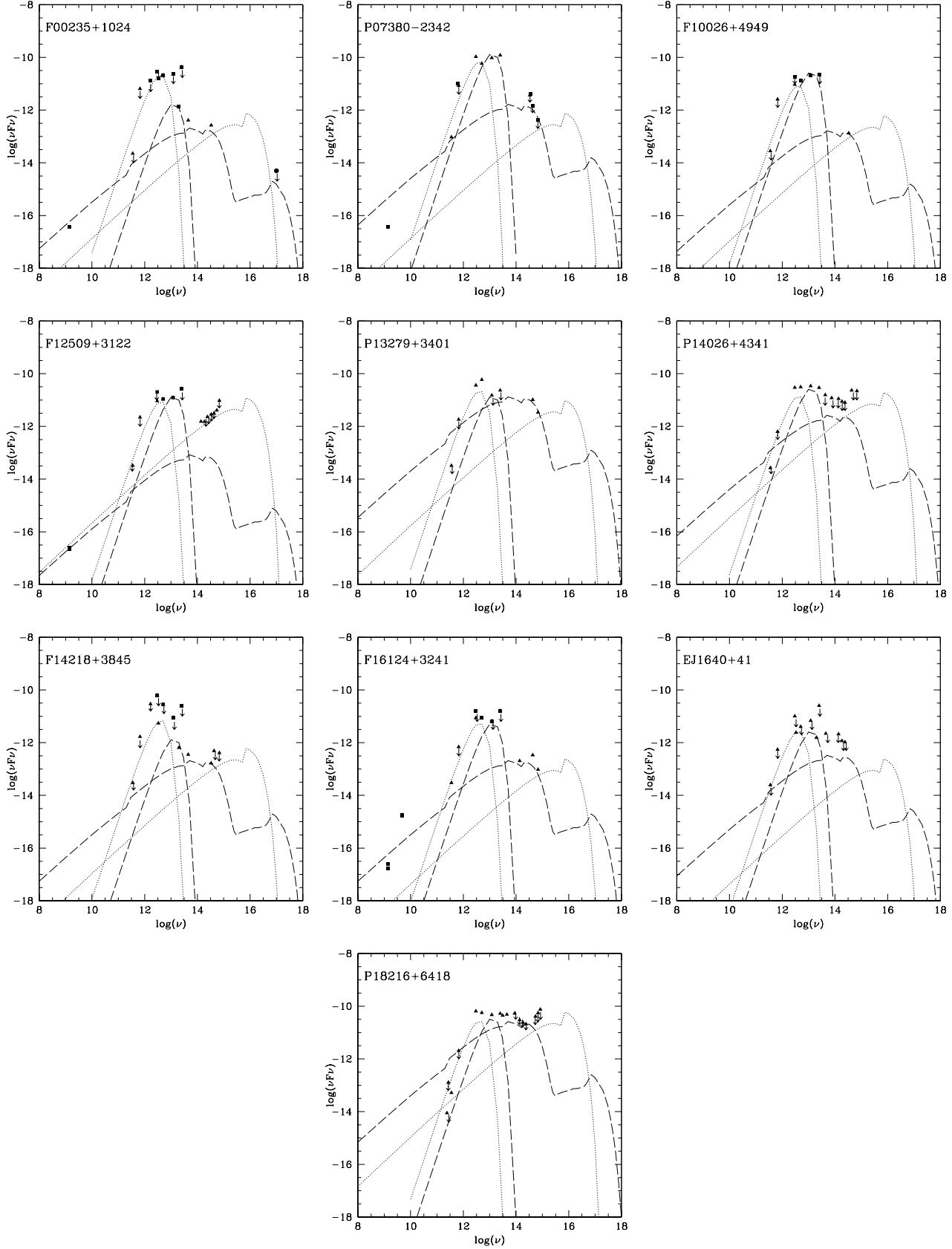


Fig. 7 Modelling the SED of the HLIRGs from the Farrah et al. (2002) sample (all fluxes at rest-frame wavelengths shortward of $4 \mu\text{m}$ are treated as upper limits due to unquantified contribution from the host galaxy). Symbols as in Fig. 5. The filled circle represents the upper limit datum in the X-ray range by Wilman et al. (1998).

may include different absorption/emission fluxes (Angeloni et al. 2007, in preparation).

We try to reproduce ("by eye") the largest number of data, constraining the modelling by upper limits. The curves representing dust emission and bremsstrahlung from different clouds are not summed up in the diagrams in order to compare directly each model with the dataset trend.

The old stellar population background is represented by a black body (bb) with $T \sim 3000\text{--}5000\text{ K}$. The data contaminated by different contributions of light from the stars, are nested within the bb curve, e.g. NGC 2110 (Contini & Viegas 2000), Arp 220 (Contini et al. 2004). The less contaminated data show the very bremsstrahlung from the clouds and constrain the models.

For all the galaxies, X-rays are upper limits because the fluxes are integrated on a large frequency range. The power-law trend of the data in the radio continuum of many galaxies is explained by synchrotron radiation created by the Fermi mechanism at the shock front.

The IR dust reradiation "bump" is generally complex, accounting for the contribution of different grains in different conditions.

Finally, the IR bands on top of the continuum are not included in the calculations of dust, therefore, they can be recognised comparing calculated with observed SEDs.

3.5.2 Modelling approach

Models are calculated at the nebula, while data are observed at Earth. Therefore to suite model results to the observed SED, the results must be multiplied by a factor η which accounts for the distance to Earth of the galaxy, for the distance of clouds from the galaxy centre, and for the filling factor.

To determine the dust-to-gas ratios in each cloud of a galaxy, we will use the method presented for the starburst regions in luminous infrared galaxies by Contini & Contini (2003). Dust and gas are coupled throughout the shock front and downstream in each cloud and the IR flux from dust is consistently calculated with bremsstrahlung, so the η factors corresponding to IR emission by dust and to bremsstrahlung must be equal. The η is determined by fitting the bremsstrahlung which extends from radio to X-rays. To recover the same η for the IR bump, we change the d/g input parameter, which affects directly dust reradiation. These changes, however, must account for the multi-cloud model.

This procedure is straightforward, but not trivial because changing the d/g ratio by a factor ≥ 10 leads to a different SED of the bremsstrahlung. Therefore the d/g ratios result from cross-checking the dust reprocessed radiation by the bremsstrahlung, for each cloud in every galaxy.

4 Results

The results of modelling of the continuum SEDs of LIRGs, ULIRGs, and of HLIRG are presented in the following sec-

tions. For most objects one type of clouds is not enough to explain the whole dataset from FIR to near-IR.

4.1 LIRGs

The modelling of LIRG is shown in Fig. 5. The data (see Appendix) come from the NED. These data are generally corrected for galactic reddening, however, background stars are included in the galaxy field and corrections have not been applied (see e.g. Code & Welch, 1982).

A deep feature at $\sim 10\text{ }\mu\text{m}$ indicates strong absorption by silicates, particularly for in NGC 253, IC 342, M 82, NGC 5236, and NGC 5253. For NGC 5236 and NGC 7552 there is also evidence of PAH emission in the mid-IR.

The wide peak in the IR, observed in all the galaxies except NGC 4038/4039, can be explained by the sum of at least two models corresponding to different shock velocities. The emission which peaks longward of $95\text{ }\mu\text{m}$ corresponds to low-velocity shocks ($V_s = 100\text{--}200\text{ km s}^{-1}$), which leads to maximum grain temperatures of $\sim 50\text{ K}$, while the emission which peaks at $\sim 30\text{ }\mu\text{m}$ corresponds to relatively high velocity shocks ($\geq 300\text{ km s}^{-1}$) with maximum grain temperatures of $\sim 120\text{ K}$. We have tried to obtain an agreement with the data within the observational error ($\leq 30\%$). For some galaxies the data are insufficient to constrain the models and clouds with $V_s = 500\text{ km s}^{-1}$ cannot be excluded. However, they correspond to lower relative contributions. These results are consistent with those found for starbursts and LIRGs by Contini & Contini (2003).

Fig. 5 shows that the IR reradiation by dust of NGC 253, IC 342, NGC 3256, NGC 3690, NGC 5236, and NGC 7552 can be also modelled by a unique model corresponding to a AGN with $V_s = 1000\text{ km s}^{-1}$, $n_0 = 1000\text{ cm}^{-3}$, and a power-law flux with $\log F_h = 11$ (model m7) as was found in Arp 220 (Contini et al. 2004, Fig. A1). Indeed, the IR emission extends all over the IR wavelength range because the grains are heated to high temperatures in the immediate post-shock region. The grains are large enough ($a_{gr} = 1\text{ }\mu\text{m}$) to survive sputtering, and they are heated to temperatures of $\sim 50\text{ K}$ by the radiation flux from the active center on the opposite side of the cloud (Fig. 2). Consider for instance NGC 253, besides the good agreement to the small aperture data by the AGN model in the optical range and by the low velocity model (m1) in the UV, we must account also for the data observed with large apertures which are explained by a starburst model (m4).

Synchrotron emission in the radio is observed in all the galaxies, except IC 342, II ZW 40, and NGC 5253. Free-free continuum absorption is evident in a few objects (NGC 3256, NGC 3690, NGC 7552).

The hybrid nature of LIRGs (starburst+AGN) appears in about half of the objects. (see Table 3).

4.2 ULIRGs

Rigopoulou et al. (1999) present, in their Table 1, ISO PHOT-S spectroscopy for a sample of ULIRGs. We have selected

Table 3 $\text{Log}(\eta)^a$ and the relative contribution of the different clouds, W_i for LIRGs

	<i>under-gal</i>		<i>starbursts</i>			<i>winds</i>		<i>AGN</i>
	m0	m1	m2	m3	m4	m5	m6	m7
NGC 253	-	-4.35	-	-	-11.4	-	-11.9	-12.1
opt	0.0	0.0831	0.0	0.0	0.191	0.0	0.0	0.726
UV	0.0	0.170	0.0	0.0	0.088	0.0	0.0	0.742
X-ray	0.0	0.611	0.0	0.0	0.0228	0.0	0.331	0.0344
IR _d	0.0	0.238	0.0	0.0	0.515	0.0	0.0	0.231
IC 342	-	-	-11.	-	-11.1	-	-11.8	-12.5
opt	0.0	0.0	0.0173	0.0	0.115	0.0	0.0	0.868
UV	0.0	0.0	0.0012	0.0	0.0561	0.0	0.0	0.943
X-ray	0.0	0.0	0.0016	0.0	0.0104	0.0	0.957	0.0314
IR _d	0.0	0.0	0.499	0.0	0.264	0.0	0.0	0.237
IIZW40	-	-6.6	-	-	-12.4	-	-	-
opt	0.0	0.196	0.0	0.0	0.804	0.0	0.0	0.0
UV	0.0	0.521	0.0	0.0	0.479	0.0	0.0	0.0
X-ray	0.0	0.938	0.0	0.0	0.0622	0.0	0.0	0.0
IR _d	0.0	0.207	0.0	0.0	0.793	0.0	0.0	0.0
M82	-	-5.	-	-	-11.8	-	-11.5	-
opt	0.0	0.709	0.0	0.0	0.290	0.0	0.0	0.0
UV	0.0	0.915	0.0	0.0	0.0841	0.0	0.001	0.0
X-ray	0.0	0.141	0.0	0.0	0.001	0.0	0.858	0.0
IR _d	0.0	0.722	0.0	0.0	0.278	0.0	0.0	0.0
NGC3256	-	-6.	-	-	-11.	-	-12.2	-12.5
opt	0.0	0.0055	0.0	0.0	0.142	0.0	0.0	0.853
UV	0.0	0.012	0.0	0.0	0.0688	0.0	0.0	0.919
X-ray	0.0	0.0687	0.0	0.0	0.0288	0.0	0.834	0.0687
IR _d	0.0	0.0235	0.0	0.0	0.571	0.0	0.0	0.406
NGC3690	-	-6.	-	-	-11.2	-	-13.	-12.8
opt	0.0	0.0105	0.0	0.0	0.171	0.0	0.0	0.818
UV	0.0	0.023	0.0	0.0	0.0841	0.0	0.0	0.893
X-ray	0.0	0.271	0.0	0.0	0.0716	0.0	0.521	0.136
IR _d	0.0	0.0401	0.0	0.0	0.613	0.0	0.0	0.347
NGC4945	-	-	-10.2	-	-10.7	-	-12.2	-
opt	0.0	0.0	0.27	0.0	0.72	0.0	0.0	0.0
UV	0.0	0.0	0.050	0.0	0.94	0.0	0.0	0.0
X-ray	0.0	0.0	0.0243	0.0	0.0628	0.0	0.913	0.0
IR _d	0.0	0.0	0.82	0.0	0.17	0.0	0.0	0.0
NGC5236	-	-4.8	-	-	-10.9	0	-12.1	-12.3
opt	0.0	0.0538	0.0	0.0	0.11	0.0	0.0	0.83
UV	0.0	0.10	0.0	0.0	0.050	0.0	0.0	0.85
X-ray	0.0	0.477	0.0	0.0	0.0159	0.0	0.460	0.0477
IR _d	0.0	0.21	0.0	0.0	0.41	0.0	0.0	0.37
NGC5253	-	-5.1	-	-	-11.7	-	-13.2	-
opt	0.0	0.607	0.0	0.0	0.39	0.0	0.0	0.0
UV	0.0	0.87	0.0	0.0	0.12	0.0	0.0	0.0
X-ray	0.0	0.860	0.0	0.0	0.00904	0.0	0.131	0.0
IR _d	0.0	0.62	0.0	0.0	0.37	0.0	0.0	0.0
NGC7552	-	-	-	-11.5	-10.8	-	-13.	-12.7
opt	0.0	0.0	0.0	0.011	0.29	0.0	0.0	0.69
UV	0.0	0.0	0.0	0.0	0.15	0.0	0.0	0.84
X-ray	0.0	0.0	0.0	0.0059	0.205	0.0	0.594	0.195
IR _d	0.0	0.0	0.0	0.47	0.41	0.0	0.0	0.11

^a in the first row of each galaxy

Table 4 $\text{Log}(\eta)^a$ and the relative contribution of the different clouds, W_i for ULIRGs

	<i>under-gal</i>		<i>starbursts</i>				<i>winds</i>	<i>AGN</i>
	m0	m1	m2	m3	m4	m5	m6	m7
MRK1014	-	-7.	-	-	-	-12.9	-12.	-
opt	0.0	0.16	0.0	0.0	0.0	0.83	0.0044	0.0
UV	0.0	0.33	0.0	0.0	0.0	0.65	0.012	0.0
X-ray	0.0	0.0051	0.0	0.0	0.0	0.0149	0.98	0.0
IR _d	0.0	0.019	0.0	0.0	0.0	0.98	0.0	0.0
UCG5101	-9.1	-	-	-	-	-13.3	-	-13.7
opt	0.0033	0.0	0.0	0.0	0.0	0.02	0.0	0.97
UV	0.0047	0.0	0.0	0.0	0.0	0.015	0.0	0.98
X-ray	0.0	0.0	0.0	0.0	0.0	0.649	0.0	0.351
IR _d	0.0078	0.0	0.0	0.0	0.0	0.64	0.0	0.35
MRK231	-8.	-	-	-	-	-11.8	-	-13.4
opt	0.016	0.0	0.0	0.0	0.0	0.24	0.0	0.74
UV	0.024	0.0	0.0	0.0	0.0	0.19	0.0	0.78
X-ray	0.0	0.0	0.0	0.0	0.0	0.967	0.0	0.033
IR _d	0.0046	0.0	0.0	0.0	0.0	0.96	0.0	0.033
MRK273	-	-	-	-	-	-12.9	-	-13.5
opt	0.0	0.0	0.0	0.0	0.0	0.031	0.0	0.97
UV	0.0	0.0	0.0	0.0	0.0	0.024	0.0	0.97
X-ray	0.0	0.0	0.0	0.0	0.0	0.745	0.0	0.255
IR _d	0.0	0.0	0.0	0.0	0.0	0.74	0.0	0.25
Arp 220	-	-9.1	-	-	-	-13.3	-	-12.9
opt	0.0	0.0001	0.0	0.0	0.0	0.007	0.0	0.99
UV	0.0	0.0003	0.0	0.0	0.0	0.003	0.0	0.997
X-ray	0.0	0.0	0.0	0.0	0.0	0.23	0.0	0.77
IR _d	0.0	0.001	0.0	0.0	0.0	0.22	0.0	0.78
NCG6240	-	-	-	-	-	-	-12.4	-13.
opt	0.0	0.0	0.0	0.0	0.0	0.0	0.0	1.0
UV	0.0	0.0	0.0	0.0	0.0	0.0	0.0	1.0
X-ray	0.0	0.0	0.0	0.0	0.0	0.0	0.960	0.0397
IR _d	0.0	0.0	0.0	0.0	0.0	0.0	0.15	0.85

^a in the first row of each galaxy

those which have a rich number of data from the NED (see Appendix), and we have added the two data points at 5.9 and 7.7 μm reported by Rigopoulou et al. (1999).

In the absence of MIR spectroscopy for ULIRGs and HLIRGs we assume the same grid of models used for LIRGs are suitable for modelling systems of higher luminosity. The results are shown in Fig. 6.

For all the galaxies of the ULIRG sample, except Mrk 1014, the low d/g clouds (m1) which significantly contribute in the LIRGs are not found, while an AGN nucleus is revealed by modelling the IR prominent flux. Free-free continuum self-absorption is evident in NGC 1014 and Mrk 231.

4.3 HLIRGs

At the brightest end of the luminous IR galaxy population lie the HLIRGs, with $L_{\text{IR}} > 10^{13} h_{65}^{-2} L_{\odot}$ (Rowan-Robinson 2000; Farrah et al. 2002; Sanders & Mirabel 1996; Tran et al. 2001; Verma et al. 2002). They claim that these objects may reveal an entirely new class of IR-emitter objects.

Farrah et al. (2002) present sub-millimetre photometry for eleven HLIRGs and use models by Efstathiou, Rowan-Robinson, & Siebenmorgen (2000) for starbursts and by Efstathiou & Rowan-Robinson (1995) for AGNs to examine the nature of the IR emission. Dust composition for starbursts is given by the dust grain model of Siebenmorgen & Krugel (1992) and by the multigrain dust model of Rowan-Robinson (1992). Farrah et al. (2002) found that AGN and starburst luminosities correlate, suggesting that a common physical factor, plausibly the dust mass, governs the luminosities of starbursts and AGNs in HLIRGs.

The models we use here are different due to the important role of collisional processes. The results of our modelling are shown in Fig. 7. We found that the IR flux can be explained by two types of clouds, one corresponding to low $V_s - n_0$ values, low U , and low d/g , (m1) while the second type of clouds corresponds to rather high velocities $V_s = 500 \text{ km s}^{-1}$, high d/g values, and a high ionization parameter U , (m5). The models correspond to $T_d(\text{max})$ of $\sim 50 \text{ K}$ and 120 K , respectively. The X-ray upper limit for the HLIRG F00235+1024 (Wiman et al 1998) integrated in

Table 5 $\text{Log}(\eta)^a$ and the IR_d relative contribution of the different clouds, W_i for HLIRGs

	<i>under-gal</i>		<i>starbursts</i>				<i>winds</i>	<i>AGN</i>
	m0	m1	m2	m3	m4	m5	m6	m7
F00235+1024	-	-7.9	-	-	-	-14.6	-	-
IR_d	0.	0.11	0.	0.	0.	0.89	0.	0.
07380-2342	-	-7.9	-	-	-	-13.7	-	-
IR_d	0.	0.01	0.	0.	0.	0.98	0.	0.
F10026+4949	-	-8.	-	-	-	-14.7	-	-
IR_d	0.	0.11	0.	0.	0.	0.89	0.	0.
F12509+3122	-	-6.7	-	-	-	-15.	-	-
IR_d	0.	0.84	0.	0.	0.	0.16	0.	0.
13279+3401	-	-6.8	-	-	-	-12.8	-	-
IR_d	0.	0.05	0.	0.	0.	0.95	0.	0.
14026+4341	-	-6.5	-	-	-	-13.5	-	-
IR_d	0.	0.21	0.	0.	0.	0.79	0.	0.
F14218+3845	-	-8.	-	-	-	-14.6	-	-
IR_d	0.	0.09	0.	0.	0.	0.91	0.	0.
F16124+3241	-	-8.4	-	-	-	-14.6	-	-
IR_d	0.	0.04	0.	0.	0.	0.96	0.	0.
EJ1640+41	-	-8.4	-	-	-	-14.4	-	-
IR_d	0.	0.02	0.	0.	0.	0.98	0.	0.
18216+6418	-	-6.	-	-	-	-12.5	-	-
IR_d	0.	0.07	0.	0.	0.	0.93	0.	0.

^a in the first row of each galaxy

the 0.1-2.4 keV band, is well explained by model m5 calculated by $V_s=500 \text{ km s}^{-1}$. Free-free continuum absorption is evident in P070380-2342 and P18216+6418.

5 Discussion

5.1 The relative importance of the different energy sources in each galaxy

The η factors (Sect. 3.5.2) derived by modelling the SED, allow to calculate the relative contribution of AGNs, starbursts, high velocity winds, and the underlying galaxy, in the different frequency ranges Δ_ν (radio_{br} , IR_{br} , opt_{br} , UV_{br} , X_{br} , IR_d , Table 2, bottom) for each galaxy, by $W_i = (F_{\Delta_\nu})_i (\eta)_i / \sum (F_{\Delta_\nu})_i (\eta)_i$. They are given in Tables 3 and 4 for LIRGs and ULIRGs, respectively. The IR bremsstrahlung is lower by a large factor than reradiation from dust, therefore is neglected.

The IR_d contribution from the starburst clouds with different velocity is generally high, except for M82 which shows a large relative contribution from the background galaxy. The strong IR_d from the starburst dust relative to AGN depends on the different character of the flux from the external source: a power-law in the AGN and a multiple black body in the starbursts. Tables 3 and 4 show, on the other hand, that when an AGN is present, its contribution prevails in the optical and UV range, while in the X-ray the high velocity winds dominate.

Tables 3 shows that relatively low V_s - n_0 clouds ($V_s < 200 \text{ km s}^{-1}$) dominate in M82 and NGC 5253. Starburst

clouds with $V_s > 300 \text{ km s}^{-1}$ are less indicated in LIRGs. An AGN contributes to the IR by $\sim 23\%$ in NGC 253 and IC 342, by $\sim 40\%$ in NGC 3256, NGC 3690, and NGC 5236. In ULIRGs (Table 4) the AGN is always present (except for Mrk 1014) and dominates by $\geq 75\%$ in Arp 220 and NGC 6240.

In Table 5 the relative contribution to the IR fluxes are given for HLIRGs. Most of the data in Fig. 6 are upper limits, so we focus on the IR. HLIRGs are modelled by two types of clouds. The relative contribution to IR_d of clouds with $V_s=500 \text{ km s}^{-1}$ (m5) is $\geq 90\%$ for all the galaxies of the sample, except for F12509+3122 which shows a large contribution from the underlying galaxy (m1).

5.2 The distance of the emitting clouds from the galaxy center

We have found by modelling the SEDs that the η factors corresponding to models m0 and m1 are higher than those corresponding to models m2-m7 by factors of $10^6 - 10^7$. This can be explained by larger distances of the clouds from the galaxy centre, and/or by a large number ($N \sim 1/\text{ff}$ where ff is the filling factor) of low V_s - n_0 clouds. The explanations are both valid. Indeed, low V_s - n_0 clouds (models m0 and m1) with d/g ratios even lower than those of the Galactic ISM (Table 2) are characteristic of the extended underlying galaxy and low V_s ($< 200 \text{ km s}^{-1}$) - n_0 ($\sim 100 \text{ cm}^{-3}$) clouds were found in the outer narrow line region of AGNs which may also contain starburst regions (Contini et al. 2002).

Table 6 The distances of the clouds (in pc) from the center of each galaxy

	<i>under-gal</i>		<i>starbursts</i>				<i>winds</i>	<i>AGN</i>	<i>radio</i>
	m0	m1	m2	m3	m4	m5	m6	m7	m_{syn}
LIRGs :									
NGC 253	-	220	-	-	20.4		3.63	2.9	141.3
IC 342	-	-	1.4	-	1.26	-	0.56	0.28	6.3
II Zw 40	-	52	-	-	6.6	-	-	-	-
M82	-	85	-	-	10.7	-	4.8	-	141.
NGC 3256	-	370	-	-	85.1	-	30.2	21.4	631.
NGC 3690	-	420	-	-	100.	-	13.2	16.6	933.
NGC 4038/4039	-	-	-	-	-	-	12.3	-	275.4
NGC 4945	-	-	59.6	-	33.1	-	5.95	-	331.
NGC 5236	-	270	-	-	24.5	-	6.16	4.9	173.7
NGC 5253	-	150	-	-	7.58	-	1.35	-	-
NGC 7552	-	-	-	37.6	84.1	-	6.68	9.44	237.1
ULIRGs :									
Mrk 1014	-	2000.	-	-	-	229.	653.	58.2	518.8
UGC 5101	45	-	-	-	-	35.5	-	22.38	-
Mrk 231	170	-	-	-	-	211.	-	33.5	1.7e3
Mrk 273	-	-	-	-	-	52.5	-	26.3	1.05e3
Arp 220	-	2029.	-	-	-	16.11	-	25.	-
NGC 6240	-	-	-	-	-	-	60.25	30.2	-
HLIRGs :									
F00235+1024	-	2600	-	-	-	113.5	-	-	-
07380-2342	-	1300	-	-	-	164.	-	-	-
F10026+4949	-	4500	-	-	-	199.	-	-	-
F12509+3122	-	14000	-	-	-	100.	-	-	-
13279+3401	-	6760	-	-	-	676.	-	-	-
14026+4341	-	7200	-	-	-	229.	-	-	-
F14218+3845	-	4800	-	-	-	245.	-	-	-
F16124+3241	-	2100	-	-	-	173.8	-	-	-
EJ1640+41	-	2780	-	-	-	278.	-	-	-
18216+6418	-	11800	-	-	-	668.	-	-	-

We define $\eta = (d_c/d)^2 (1/\mathcal{f}\mathcal{f})$, where d is the distance of the galaxy to Earth and d_c the distance of clouds from the galaxy center. Fragmentation by shocks leads to clouds with different geometrical thickness, D (Table 2), particularly low in the underlying galaxy. We adopt $\mathcal{f}\mathcal{f} \sim D_{min}/D_{max} = 10^{-4}$ (D_{min} and D_{max} are the minimum and maximum geometrical thickness of the clouds in Table 2) for the underlying galaxy clouds (m0 and m1), and $\mathcal{f}\mathcal{f} \sim 1$ for the starburst and AGN clouds (m2-m7).

Models m6 and m7 with a high shock velocity ($V_s = 1000 \text{ km s}^{-1}$) explain the observed soft X-rays, which are upper limits. Dust emission calculated by model m7, which appears in most of the ULIRGs, explains the mid- to far-IR flux observed in some galaxies. The η of models m6 and m7 are relatively low indicating that the high V_s clouds are located closer to the centre.

The distances of the clouds from the galaxy center are shown in Table 6. We have found by fitting the continuum SED of LIRGs that a large number of low V_s , n_0 clouds are located in the outskirts of the galaxies. Even adopting the low $\mathcal{f}\mathcal{f}$ indicated above, the distance of these clouds from the center results higher by a factor ≥ 10 than that of clouds

corresponding to higher velocities and densities. The large regions of low V_s - n_0 clouds with low d/g are less evident in ULIRGs, as high and low velocity clouds coexist because merging leads to fragmentation and mixing. Indeed, the galaxies selected from the Rigopoulou et al. (1999) sample are few but they all show an irregular morphology due to merging (e.g. Leech et al 1994). Table 6 shows that the average distances of the starburst clouds from the centre is similar for LIRGs and ULIRGs, within 100 pc for almost all galaxies, except for Mrk 1014. The luminous IR galaxies of the Verma et al sample, with $L_{IR} > 10^{11} L_\odot$, NGC 3256 and NGC 3690 which are identified as a colliding pair and a peculiar merger, respectively, show starburst cloud distances from the centre ~ 100 pc. There are not enough data to model the NCG 4038/4039 interacting complex.

HLIRG redshifts (Farrah et al. 2002, table 1 and references therein) are higher than those of LIRGs, leading to distances larger by factors of 100- 1000. We have found (Table 6, bottom) that d_c should be higher for HLIRGs than for LIRGs by about a factor > 10 in average, adopting the same $\mathcal{f}\mathcal{f}$ which were used for the other galaxy samples. To recover the dimensions of the extended region of the other galaxies,

Table 7 Dust-to-gas ratios (in units of 4×10^{-4}) in each galaxy

	<i>under-gal</i>		<i>starbursts</i>				<i>winds</i>	<i>AGN</i>
	m0	m1	m2	m3	m4	m5	m6	m7
LIRGs :								
NGC 253	-	0.70	-	-	100	-	100	200
IC 342	-	-	100	-	100	-	100	250
II Zw 40	-	0.75	-	-	158	-	-	-
M82	-	6.	-	-	340	-	100	-
NGC 3256	-	4.7	-	-	200	-	100	63.
NGC 3690	-	3	-	-	100	-	100	79.
NGC 4038/9	-	-	-	-	-	-	100	-
NGC 4945	-	-	100	-	100	-	100	-
NGC 5236	-	0.75	-	-	100	-	100	126.
NGC 5253	-	0.24	-	-	100	-	100	-
NGC 7552	-	-	-	8.	20.	-	100	79.
ULIRGs :								
Mrk 1014	-	0.95	-	-	-	5.	-	-
UGC 5101	6.	-	-	-	-	30.	-	100.
Mrk 231	0.16	-	-	-	-	4.	-	126.
Mrk 273	-	-	-	-	-	5.	-	100
Arp 220	-	0.15	-	-	-	50.	-	100
NGC 6240	-	-	-	-	-	-	20	31.6
HLIRGs :								
F00235+1024	-	2.4	-	-	-	5.	-	-
07380-2342	-	7.5	-	-	-	50.	-	-
F10026+4949	-	1.2	-	-	-	100.	-	-
F12509+3122	-	0.06	-	-	-	100.	-	-
13279+3401	-	0.19	-	-	-	0.6	-	-
14026+4341	-	0.06	-	-	-	6.3	-	-
F14218+3845	-	0.95	-	-	-	4.	-	-
F16124+3241	-	1.9	-	-	-	16.	-	-
EJ1640+41	-	0.95	-	-	-	5.	-	-
18216+6418	-	0.04	-	-	-	0.8	-	-

^a adopting $H_0 = 75 \text{ km s}^{-1} \text{ Mpc}^{-1}$

^b 1-1000 μm luminosities obtained from the best-fitting combined starburst-AGN models (Farrah et al. 2002, table 3)

lower \mathcal{F} should be adopted. It seems that Mrk 1014 with $\log(L_{\text{IR}}/L_{\odot}) = 12.5$ has characteristics similar to HLIRGs.

Regions of 200-900 pc are generally characteristic of the NLR of objects such as QSOs, Seyfert 1, and narrow line galaxies. This indicates that also HII regions are located within the NLR of these galaxies. Synchrotron emission in the radio range corresponds to larger distances from the centre, which is reasonable enough considering that it is generally created in the lobes of extended jets.

5.3 The dust-to-gas ratios

The d/g ratios relative to those of the Galactic ISM ($\sim 4 \times 10^{-4}$ by mass) for each type of clouds in each galaxy are given in Table 7. More particularly, d/g as high as 0.1 were found in M 82, and $d/g \geq 0.04$ in the starburst clouds of most of the LIRGs. This may indicate that dust in the starburst regions of LIRGs is of SN origin. Indeed high velocity winds were found modelling the X-ray in Figs. 5. SN corresponding to explosions of 10-30 M_{\odot} stars, are potentially

the most important source of interstellar dust (Dwek 2004). The total mass of condensable elements (C, Mg, Si, S, Ca, Fe, Ni and associated O) ejected by a 30 M_{\odot} mass star is 0.3-2 M_{\odot} leading to $d/g \sim 0.01$ -0.07. Dust from red giants and AGB is less suitable to high velocity clouds. For comparison, d/g between $\sim 2.5 \times 10^{-3}$ and 6.6×10^{-3} were determined for actively star-forming galaxies by Calzetti (2000) and for PG quasars by Haas et al (2003) adopting the Hildebrand (1983) classical method.

In Table 8 dust masses, M_d , calculated in the present work are compared with those calculated by the models of Farrah et al. (2002). Discrepancies within a factor ≤ 3 are found for all the galaxies of the sample considering the errors, except for F10026+4949 and 18216+6418 where the discrepancies are greater than a factor of 10. The discrepancies depend on the fact that the dust masses were calculated by Farrah et al. with the Hildebrand (1983) method. In 18216+6418 we predict very low d/g , because large slabs of gas are deduced from the strong self-absorption of free-free

Table 8 Comparison of M_d calculated in the present work with M_d reported by Farrah et al. (2002) in HLIRGs

	M_d^1 ($10^8 M_\odot$)	M_d (Farrah et al.) ($10^8 M_\odot$)
F00235+1024	1.86	1.95
07380-2342	17.8	6.17
F10026+4949	35.	< 5
F12509+3122	6.4	1.58
13279+3401	0.22	-
14026+4341	2.0	1.74
F14218+3845	1.4	1.07
F16124+3241	6.1	3.47
EJ1640+41	1.9	<1.58
18216+6418	0.3	3.24

¹ adopting $M_{\text{gas}} = 10^{11} M_\odot$ (Farrah et al. 2002)

radiation at long wavelengths (Fig. 7, last diagram). Adopting a temperature $T=1000$ K and a density $n=10^4 \text{ cm}^{-3}$ downstream of clouds in physical conditions corresponding to $V_s=500 \text{ km s}^{-1}$ and $n_0=300 \text{ cm}^{-3}$, the gas is optically thick at $\nu \leq 300 \text{ GHz}$ for a layer $\geq 242.2 \text{ pc}$ thick (Osterbrock 1988), which is actually of the order of the calculated radius of the NLR (Table 6).

6 Summary

In this work we have modelled consistently the IR dust emission and the bremsstrahlung. From the analysis of dust-to-gas ratios in galaxies with different IR luminosities, we conclude that the high infrared luminosities generally depend on high amount of dust relative to gas close to the galaxy centre. This is revealed by the continuum emitted downstream of relatively high velocity clouds. Relatively high d/g (0.04 by mass) were found in the LIRG clouds with $V_s = 300\text{-}500 \text{ km s}^{-1}$, higher by a factor of ~ 100 than in the ISM ($\sim 4 \cdot 10^{-4}$).

Half of the LIRGs of the sample contain an AGN, which is found in almost all ULIRGs and in none of the HLIRGs.

Interestingly, we could not demonstrate that higher L_{IR} as those observed in HLIRGs correspond to higher dust-to-gas ratios. On the contrary, the highest d/g appear in LIRGs. Notice that the HLIRG types correspond to narrow-line galaxies, Seyfert 1, and QSO. It was found in previous modelling (Contini et al. 2002) that d/g ratios in the narrow line region of these galaxies are lower by a factor of ~ 10 than for Seyfert 2 and LINERs. It seems that in some HLIRGs the high IR luminosities include the contribution of bremsstrahlung from cool gas. The relatively high bremsstrahlung and the large distances of the emitting clouds from the galaxy centre suggest that the HLIRGs of the Farrah et al sample were selected among large, massive objects.

Acknowledgments

We are very grateful to an anonymous referee for helpful and valuable comments. We thank R. Angeloni for interesting conversations. This paper makes use of observations by the "Two micron all sky survey team" from NASA/IPAC Extragalactic Database.

Appendix : The references for the NED data

Fabbiano et al. (1992), Brinkmann et al. (1994), Code & Welch (1982), De Vaucouleurs et al. (1991), Lauberts & Valentijn (1989), Spinoglio et al. (1995), Glass (1973), Aaronson (1977), Jarrett et al. (2003), Aaronson et al. (1980), Rieke et al. (1975), Rieke & Lebofsky (1978), Rieke & Low (1972), Rice et al. (1988), Soifer et al. (1989), Moshir et al. (1990), Rieke et al. (1973), Hildebrand et al. (1977), Chini et al. (1994), Gelzhaier & Witzel (1981), Schimmins & Wall (1973), Wright et al. Otrupcek (1990), Whiteoak (1970), Kuhr et al. (1981), Wall et al. (1976), Condon et al. (1998), Large et al. (1991), Douglas et al. (1996), Slee (1995), Israel et al. (1990), Zwicky & Herzog (1968), Becklin et al. (1980), Becker et al. (1991), Gregory et al. (1991), Gregory & Condon (1991), White & Becker (1992), Thuan (1983), Heisler et al. (1996), Huchtmeier & Richter (1989), Rifatto et al. (1995), Donas et al. (1987), Johnson (1966), Kleinmann & Low (1970a), Kleinmann & Low (1970b), Rieke et al. (1980), Golombek et al. (1988), Laing & Peacock (1980), Genzel et al. (1976), Kuhr (1980), Pauliny-Toth et al. (1978), Kellermann et al. (1969), Kuhr et al. (1981), Condon (1983), White & Becker (1992), Pauliny-Toth & Wade (1964), Cohen et al. (1977), Kinney et al. (1993), Gregory et al. (1994), Huchra (1977), Joyce & Simon (1976), Allen (1976), Lebofsky & Rieke (1979), Soifer et al. (2001), Carico et al. (1972), Griffith et al. (1994), Mathewson & Ford (1996), Wright et al. (1994), Jones & McAdam (1992), Mauch et al. (1992), Mauch (2003), Dyck et al. (1978), De Vaucouleurs & Longo (1988), Glass (1976), Ward et al. (1982), Rousset et al. (2001), Frogel et al. (1982), Wright et al. (1966), White et al. (2000), Moorwood & Glass (1982), Rieke (1976), Kleinmann & Wright (1974), Knapp (1994), Griessmith et al. (1982), Surace & Sanders (2000), Maddox et al. (1990), Scoville et al. (2000), Neugebauer et al. (1987), Haas et al. (2003), Sanders et al. (1989), Barvainis & Antonucci (1989), Barvainis et al. (1996), Rigopoulou et al. (1996), Maiolino et al. (1995), Benford (1999), McAlary et al. (1979), Joyce (1975), Rieke (1976), Rieke (1978), Stein & Weedman (1976), Klaas et al. (2001), Patnaik et al. (1992), Sramek & Tovmassian (1986), Zwicky & Herzog (1966), Zwicky & Herzog (1963), Eales et al. (1989), Dunne et al. (2000), Chini et al. (1986), Condon et al. (1983), Dressel & Condon (1978), Waldrum et al. (1996), Zwicky et al. (1961), Rudy et al. (1982), Griffith et al. (1995), Gower et al. (1967), Becker et al. (1995),

References

- Aaronson, M. 1977 Harvard University Thesis
- Aaronson, M., Mould, J., & Huchra, J., 1980 ApJ, 237, 655
- Allen, C.W. 1973, Astrophysical Quantities (London: Athlon)
- Allen, D.A. 1976, ApJ, 207, 367
- Alonso-Herrero, A., Quillen, A.C., Rieke, G.H., Ivanov, V.D., & Efstathiou, A. 2003, ApJ, 126, 81
- Armus, L. et al. 2006, ApJ, 640, 204
- Barvainis, R., & Antonucci, R. 1989, ApJS, 70, 257

- Barvainis, Lonsdale, C., & Antonucci, R. 1996, *AJ*, 111, 1431
- Becker, R.W., White, R.L., & Edwards, A.L. 1991, *ApJS*, 75, 1
- Becker, R.H., White, R.L., & Helfand, D.J. 1995, *ApJ*, 450, 559
- Becklin, E.E., Gatley, I., Matthews, K., Neugebauer, G., Sellgren, K., Werner, M.W. 1980, *ApJ*, 236, 441
- Benford, D.J. 1999 California Institute of Technology, Thesis
- Borne, K.D., Keel, W.C., Appleton, P.N., Struck, C., Lucas, R.A., & Achultz, A.B. 2001, *IAU Symposium Series*, Vol. 2007, 2001, E.K. Grebel, D. Geisler, & D. Minniti eds
- Brinkmann, W., Siebert, J., & Boller, Th. 1994, *A&A*, 281, 355
- Calzetti, D., Armus, L., Bohlin, R.C., Kinney, A.L., Koornneef, J., & Storchi-Bergmann, T. 2000, 533, 682
- Carico, D.P., Keene, J., Soifer, B.T., Neugebauer, G., & Tovmasian, H. 1972, *AJ*, 77, 705
- Chini, R., Kreysa, E., Krugel, E., & Mezger, P.B. 1986, *A&A*, 166, L8
- Chini, R., Kreysa, E., Mezger, P.G., & Gennud, H-P. 1994, *A&A*, 137, 117
- Clavel, J., Shulz, B., Altieri, B. et al. 2000 *A&A*, 357, 839
- Code, A., & Welch, G. 1982, *ApJ*, 256, 1
- Cohen, A.M., Porcas, R.W., Browne, I.W.A., Daintree, E.J., & Walsh, D., 1977, *MmRAS*, 84, 1
- Condon, J.J., 1983, *ApJS*, 53, 459
- Condon, J.J., Condon, M.A., Broderick, J.J., & Davis, M.M. 1983,, *AJ*, 88, 20
- Condon, J.J., Cotton, W.D., Greisen, E.W., Yin, Q.F., Perley, P.A., Taylor, G.B., & Broderick, J.J. 1998, *AJ*, 115, 1693
- Contini, M. 2004, *A&A*, 422, 591
- Contini, M., & Contini, T. 2003, *MNRAS* 342, 299
- Contini, M., Formiggini, L. 2001, *A&A*, 375, 579
- Contini, M., & Viegas, S.M. 2000, *ApJ*, 535, 721
- Contini, M., & Viegas, S.M. 2001, *ApJS*, 132, 211
- Contini, M., & Viegas, S.M. 2001, *ApJS*, 137, 75
- Contini, M., Viegas, S.M., & Campos, P.E. 2003, *MNRAS*, 346, 37
- Contini, M., Viegas, S.M., & Prieto, M.A. 2004, *MNRAS*, 348, 1065
- Contini, M., Radovich, M., Rafanelli, P., & Richter, G.M. 2002, *ApJ*, 572, 124
- Cox, D.P. 1972, *ApJ*, 178, 143
- De Vaucouleurs, G., De Vaucouleurs, A., Corwin Jr, H.G., Buta, R.J., Paturel, G., & Fouque, P. 1991, *RC3.9.C*
- De Vaucouleurs, A., & Longo, G. 1988, *VirPh.c*
- Donas, J., Deharveng, J.M., Laget, M., Milliard, B., & Hugnercin, D. 1987, *A&A*, 180, 12
- Douglas, J.N., Bash, F.N., Bozayan, F.A., Torrence,, G.W., & Wolfe, C. 1996, *AJ*, 111, 1945
- Draine, B.T. 2003 in *The cold Universe: Saas-Fee Advancecourse* 32. ed Pfenninger, Berlin, Springer-Verlag
- Dressel, L.L., & Condon, J.J. 1978, *ApJS*, 36, 53
- Dunne, L., Eales, S., Edmunds, M., Ivison, R., Alexander, P., & Clements, D.L. 2000 *MNRAS*, 315, 115
- Dyck, H. M., Becklin, E.E., & Capps, R.W. 1978, *BAAS*, 10, 422
- Dwek, E. 1987, *ApJ*, 322, 812
- Dwek, E. 2004, *ApJ*, 607, 848
- Eales, S.A., Wynn-Williams, C.G., & Duncan, W.D. 1989, *ApJ*, 339, 859
- Edmunds, M.G. 2004, *ApJ*, 597, L33
- Efstathiou, A. & Rowan-Robinson, M. 1995, *MNRAS*, 273, 649
- Efstathiou, A., Rowan-Robinson, M. & Siebenmorgen, R. 2000, *MNRAS*, 313, 734
- Fabbiano, G., Kim, D.-W., & Trinchieri, G. 1992, *ApJS*, 80, 531
- Farrah, D., Serjeant, S., Afstathiou, A., Rowan-Robinson, M., & Verma, A. 2002, *MNRAS*, 335, 1163
- Frogel, J.F., Elias, J.H., & Phillips, V.M. 1982, *ApJ*, 260, 70
- Galliano, F. 2004, *astro-ph/0501017*
- Genzel, R., & Cesarsky, C. 2000, *ARA&A*, 38, 761
- Genzel, R., Lutz, D., Sturm, E., et al. 1998 *ApJ*, 498, 579
- Gelzhaler, B.J., & Witzel, A. 1981, *AJ*, 86, 1306
- Genzel, R., Pauliny-Toth, I.I.K., Preuss, E., Witzel, A., 1976, *AJ*, 81, 1084
- Glass, I.S. 1973, *MNRAS*, 164, 155
- Glass, I.S. 1976, *MNRAS*, 175, 191
- Golombek, D., Miley, G.K., & Neugebauer, G. 1988, *AJ*, 95, 26
- Gower, J.F.R., Scott, P.F., & Wills, D. 1967 *MmRAS*, 71, 49
- Graham, M.J., Zhang, Q 2000, *ApJS*, 127, 339
- Gregory, P.C., & Condon, J.J. 1991, *ApJS*, 75, 1011
- Gregory, P.C., Vavasour, J.D., Scott, W.K., Condon, J.J. 1994, *ApJS*, 90, 173
- Griersmith, D., Hyland, A.R., & Jones, T.J. 1982, *AJ*, 87, 1106
- Griffith, M.R., Wright, A.E., Burke, B.F., Ekers, R.D. 1994, *ApJS*, 90, 179
- Griffith, M.R., Wright, A.E., Burke, B.F., Ekers, R.D. 1995, *ApJS*, 97, 347
- Groves, B. A., Dopita, M. A., & Sutherland, R. S. 2004, *ApJS*, 153, 9
- Haas, M. et al. 2003, *A&A*, 402, 87
- Heckman, T.M., Miles, G.K., van Breugel, W.J.M., Butcher, H.R. 1981, *ApJ*, 247, 403
- Heisler, C.A., De Robertis, M.M., & Nadeau, D.. 1996, *MNRAS*, 280, 579
- Hildebrand, R.H. 1983, *QJRAS*, 24, 267
- Hildebrand, R., Whitcomb, S., Winston, S., Stiening, R., Harper, D., Moseley, S. 1977, *ApJ*, 216, 698
- Huchra, J.P. 1977, *ApJS*, 35, 171
- Huchtmeier, W.K., & Richter, O.-G., 1989 *A general Catalogue of HI observations of galaxies*, 1989, New York, Springer-Verlag
- Israel, F.P., & Mahoney, M.J. 1990 *ApJ*, 352, 30
- Jarrett, T.H., Chester, T., Cutri, R., Schneider, S.E., & Huchra, J.P. 2003, *AJ*, 125, 525
- Johnson, H.L. 1966, *ApJ*, 143, 187
- Jones, P.A., & McAdam, W.B. 1992, *ApJS*, 80, 137
- Joyce, R.R., Knacke, R.F., Simon, M., & Young, E. 1975, *PASP*, 87, 683
- Joyce, R.R., & Simon, M. 1976, *PASP*, 88, 870
- Kellermann, K.I., Pauliny-Toth, I.I.K., & Williams, P.J.S. 1969, *ApJ*, 157, 1
- Kinney, A.L., Bohlin, R.C., Calzetti, D., Panagia, N., & Wyse, R.F.G. 1993, *ApJS*, 86, 5
- Klaas, U. et al. 2001, *A&A*, 379, 823
- Kleinmann, D.E., & Low, F.J. 1970, *ApJ*, 159, L65
- Kleinmann, D.E., & Low, F.J. 1970, *ApJ*, 161, L203
- Kleinmann, D.E., & Wright, E.L. 1974, *ApJ*, 191, L19
- Knapp, J. 1994 *PrieC.U.J.*
- Kuhr, H. 1980 University of Bonn, PhD Thesis
- Kuhr, H., Witzel, A., Pauliny-Toth, I.I.K., & Nauber, U. 1981, *A&AS*, 45, 367
- Laing, R.A., & Peacock, J.A. 1980, *MNRAS*, 190, 903
- Large, M. I., Mills, B.V., Little, A.G., Crawford, D.F., & Sutton, J.M. 1991 *MNRAS*, 194, 694
- Lauberts, A., & Valentijn, E.A. 1989, *ESOLV.C*
- Laurent, O., Mirabel, I.F., Charmandaris, V., Gallais, P., Madden, S.C., Sauvage, M., Vigroux, L., & Cesarsky, C. 2000, *A&A*, 359, 887
- Lebofsky, M.J., & Rieke, G.H. 1979, *ApJ*, 229, 111

- Leech, K.J., Rowan-Robinson, M., Lawrence, A., & Hughes, J.D. 1994, *MNRAS*, 267, 253
- Lutz, D., Spoon, H.W.W., Rigopoulou, D., Moorwood, A.F.M., & Genzel, R. 1998, *ApJ*, 505, L103
- Lutz, D., Veilleux, S., & Genzel, R. 1999, *ApJ*, 517, L13
- Lutz, D. et al 2000, *ApJ*, 530, 733
- Lutz, D. et al 2000, *ApJ*, 536, 697
- Maddox, S.J., Sutherland, W.J., Efstathiou, G., & Loveday, J. 1990 *MNRAS*, 243, 692
- Maiolino, R., Ruiz, M., Rieke, G.H., & Keller, L.D. 1995, *ApJ*, 446, 561
- Mathewson, D.S., & Ford, V.L. 1996, *ApJS*, 107, 97
- Mauch, T., Murphy, T., Buttery, H.J., Curran, J., Hursthead, R.W., Piestrzynsky, B., Robertson, J.G., Sadler, E. M. 2003, *MNRAS*, 342, 1117
- McAlary, C.W., McLaren, R.A., & Crabtree, D.R. 1979, *ApJ*, 234, 471
- Moorwood, A.F.M., & Glass, I.S. 1982, *A&A*, 115, 84
- Moshir, M. et al. 1990 *IRASFC*
- Neugebauer, G., Green, R.F., Matthews, K., Schmidt, M., Soifer, B.T., & Bennett, J. 1987, *ApJS*, 63, 615
- Osterbrock, D.E. 1988 in 'Astrophysics of gaseous nebulae and active galactic nuclei', University Science Books
- Patraik, A.R., Browne, I.W.A., Wilkinson, P.N., & Wrobel, J.M. 1992, *MNRAS*, 254, 655
- Pauliny-Toth, I.I.K., & Wade, C.M. 1964, *AJ*, 69, 277
- Pauliny-Toth, I.I.K., Witzel, A., Preuss, E., Kuhr, H., & Kellermann, K.I. 1978, *AJ*, 83, 451
- Peeters, E., Spoon, H.W.W., & Tielens, A.G.G.M. 2004, *astro-ph/0406183*
- Polatidis, A.G., & Conway, J.E. 2004, *Proceedings of the 7th VLBI Network Symposium*. Bachiller, R., Colomer, F., Desmurs, J.F., de Vicente, P. (eds).
- Rice, W., Lonsdale, C.J., Soifer, B.T., Neugebauer, G., Kopan, E.L., Lloyd, L.A., De Jong, T., Habing, H.J. 1988, *ApJS*, 68, 91
- Rieke, G.H. 1976, *ApJ*, 210, L5
- Rieke, G.H. 1978, *ApJ*, 226, 550
- Rieke, G.H., & Lebofsky, M.J. 1978, *ApJ*, 220, L37
- Rieke, G.H., Lebofsky, M.J., Thompson, R.I., Low, F.J., & Tokunaga, A.T. 1980, *ApJ*, 238, 24
- Rieke, G.H., & Low, F.J. 1972 *ApJ*, 176, L95
- Rieke, G.H., & Low, F.J. 1975, *ApJ*, 197, 17
- Rieke, G.H. 1976 *ApJ*, 206, L15
- Rieke, G.H., Harper, D.A., Low, F.J., & Armstrong, K.R. 1973, *ApJ*, 183, L67
- Rifatto, A., Longo, G., & Capaccioli, M. 1995, *A&AS*, 114, 527
- Rigopoulou, D., Spoon, H.W.W., Genzel, R., Lutz, D., Moorwood, A.F.M., & Tran, Q.D. 1999 *ApJ*, 118, 2625
- Rigopoulou, D., Lawrence, A., & Rowan-Robinson, M. 1996, *MNRAS*, 278, 1049
- Rudy, R.J., Levan, P.D., & Rodriguez-Espinosa, J.M. 1982, *AJ*, 87, 598
- Roussel, H. et al. 2001, *A&A*, 369, 473
- Rowan-Robinson, M. 1992, *MNRAS*, 252, 787.
- Rowan-Robinson, M. 2000, *MNRAS*, 316, 885.
- Sanders, D.B., & Mirabel, I.F. 1996, *ARA&A*, 34, 749
- Sanders, D.B., Phinney, E.S., Neugebauer, G., Soifer, B.T., & Matthews, K. 1989, *ApJ*, 347, 29
- Schimmins, A.J., & Wall, J.V. 1973, *AuJPh*, 26, 93
- Scoville, N.Z., et al. 2000, *AJ*, 119, 991
- Schneider, R., Ferrara, A., & Salvaterra, R. 2004, *MNRAS*, 351, 1386
- Siebenmorgen, R. & Krugel, E. 1992, *A&A*, 259, 614
- Silva, L., Granato, G.L., Bressan, A., Danese, L. 1998, *ApJ*, 509, 103
- Slee, O. 1995, *AuJPh*, 48, 143
- Soifer, B.T., Boehmer, L., Neugebauer, G., & Sanders, D.B. 1989, *AJ*, 98, 766
- Soifer, B.T., et al. 2001, *AJ*, 122, 1213
- Spinoglio, L., Malkan, M.A., Rush, B., Carrasco, L., & Recillas-Cruz, E. 1995, *ApJ*, 453, 616
- Spoon, H.W.W., Keane, J.V., Tielens, A.G.G.M., Lutz, D., Moorwood, A.F.M., & Laurent, O. 2002, *A&A*, 385, 1022
- Sramek, R., & Tovmassian, H. 1986, *ApJ*, 207, 725
- Stein, W.A., & Weedman, D.W. 1976, *ApJ*, 205, 44
- Sturm, E. et al. 2002, *AAS*, 201, 4806
- Sturm, E. et al. 2005, *ApJ*, 629, L21
- Surace, J.A., & Sanders, D.B. 2000, *AJ*, 120, 604
- Thuan, T.X. 1983, *ApJ*, 268, 667
- Tran, Q.D. et al 2001, *ApJ*, 552, 527
- Verma, A., Rowan-Robinson, M., McMahon, R., & Efstathiou, A. 2002, *MNRAS*, 335, 574
- Verma, A., Lutz, D., Sturm, E., Sternberg, A., Genzel, R., & Vacca, W. 2003, *A&A*, 403, 829
- Verma, A., Charmandaris, V., Klaas, U., Lutz, D., Haas, M. 2005 *astro-ph/0507165*
- Viegas, S.M., & Contini, M. 1994, 428, 113
- Viegas, S.M., Contini, M., & Contini, T. 1999, *A&A*, 347, 112
- Waldram, E.M., Yates, J.A., Riley, J.M., & Warner, P.J. 1996, *MNRAS*, 282, 779
- Wall, J.V., Wright, A.E., & Bolton, J.G., 1976, *AuJPA*, 39, 1
- Ward, M., Allen, D.A., Wilson, A.S., Smith, M.G., & Wright, A.E. 1982, *MNRAS*, 199, 953
- Weedman, D.W. et al. 2005, *ApJ*, 633, 706
- White, R.L., & Becker, R.H. 1992, *ApJS*, 98, 331
- White, N.E. Giommi, P., & Angelini, L. 2000 *WGA.C*
- Whiteoak, J.B. 1970 *ApL*, 5, 29
- Whittet, D.C., 1992, *Dust in the Galactic Environment*, IOP Publishing, Bristol
- Wiman, R.J., Fabian, A.C., Cutri, R.M., Crawford, C.S., & Brandt, W.N. 1998, *MNRAS*, 300, L7
- Wright, A.E., Griffith, M.P., Hunt, A.J., Trough, E., Butkee, B.F., Ekers, R.D. 1966, *ApJS*, 103, 145
- Wright, A.E., Griffith, M.R., Burke, B.F., & Ekers, R.D. 1994, *ApJS*, 91, 111
- Wright, A., & Otrupcek, R. 1990, *Parkes Catalogue*, 1990 Australian Telescope National Facility
- Zwicky, F., & Herzog, E. 1963, *CGCG2.C*
- Zwicky, F., & Herzog, E. 1966 *CGCG3.C*
- Zwicky, F., & Herzog, E. 1968 *CGCG4.C*, *Catalogue of Galaxies and of Clusters of Galaxies IV*
- Zwicky, F., Herzog, E., & Wild, P. 1961, *CGCG1.C*